

Primordial Black Holes: Observational Characteristics of The Final Evaporation

T. N. Ukwatta^a, D. R. Stump^b, J. T. Linnemann^b, J. H. MacGibbon^c, S. S. Marinelli^b, T. Yapici^b, K. Tollefson^b

^a*Director's Postdoctoral Fellow, Space and Remote Sensing (ISR-2), Los Alamos National Laboratory, Los Alamos, NM 87545, USA.*

^b*Department of Physics and Astronomy, Michigan State University, East Lansing, MI 48824, USA.*

^c*Department of Physics, University of North Florida, Jacksonville, FL 32224, USA.*

Abstract

Many early universe theories predict the creation of Primordial Black Holes (PBHs). PBHs could have masses ranging from the Planck mass to 10^5 solar masses or higher depending on the size of the universe at formation. A Black Hole (BH) has a Hawking temperature which is inversely proportional to its mass. Hence a sufficiently small BH will quasi-thermally radiate particles at an ever-increasing rate as emission lowers its mass and raises its temperature. The final moments of this evaporation phase should be explosive and its description dependent on the particle physics model. In this work we investigate the final few seconds of BH evaporation using the Standard Model of particle physics incorporating the most recent LHC results and calculate energy dependent PBH burst light curves in the GeV/TeV energy range. Moreover, we explore PBH burst search methods and potential observational PBH burst signatures relevant to very high energy gamma-ray observatories.

Keywords: Primordial Black Holes

1. Introduction

Many current theories of the early universe predict the production of primordial black holes (PBHs)[1]. Cosmological density fluctuations and other mechanisms such as those associated with phase transitions in the early universe could have created PBHs with masses of order of, or smaller than, the

cosmological horizon size at the time of formation. Depending on the formation mechanism, PBHs could form at times from the Planck time¹ to 1 second after the Big Bang, or later. Hence the initial mass of a PBH could be as small as the Planck mass² or as massive as 10^5 solar mass, or higher.

In 1974, Hawking showed by convolving quantum field theory, thermodynamics and general relativity that a Black Hole (BH) has a temperature inversely proportional to its mass and emits photon and particle radiation with thermal spectra [2]. As the BH emits this radiation, its mass decreases and hence its temperature and flux increase. A PBH that formed with an initial mass of $\sim 5.0 \times 10^{11}$ kg in the early universe should be expiring today [3] with a burst of high-energy particles, including gamma-rays in the MeV to TeV energy range. Thus PBHs are candidate gamma-ray burst (GRB) progenitors [4].

Confirmed detection of a PBH evaporation event would provide valuable insights into many areas of physics including the early universe, high energy particle physics and the convolution of gravitation with thermodynamics. Conversely, non-detection of PBH evaporation events in sky searches would place important limits on models of the early universe. One of the most important reasons to search for PBHs is to constrain the cosmological density fluctuation spectrum in the early universe on scales smaller than those constrained by the cosmic microwave background. There is particular interest in whether PBHs form from the quantum fluctuations associated with many different types of inflationary scenarios [1]. Detection or upper limits on the number density of PBHs can thus inform inflationary models.

PBHs may be detectable by virtue of several effects. For example, PBHs with planetary-scale masses may be detectable by their gravitational effects in micro-lensing observations [5]; or accretion of matter onto PBHs in relatively dense environments may produce distinct, observable radiation [6]. Such situations, however, should be rare and therefore difficult to use as probes of the cosmological or local PBH distribution. On the other hand, any PBHs with an initial mass of $\sim 5.0 \times 10^{11}$ kg should be expiring today in a final burst of Hawking radiation. These events, out to a determinable distance, should be detectable at Earth as sudden bursts of gamma-rays in the sky. Many gamma-ray observatories have performed searches for such events [7;

¹Planck time $(\hbar G/c^5)^{1/2} \simeq 5.391 \times 10^{-44}$ s

²Planck mass $(\hbar c/G)^{1/2} \simeq 2.176 \times 10^{-8}$ kg

8; 9; 10; 11; 12; 13].

The properties of the BH final burst depend on the physics governing the production and decay of high-energy particles. As the BH evaporates and loses mass over its lifetime, its temperature increases. The higher the number of fundamental particle degrees of freedom, the faster and more powerful will be the final burst from the BH. The details of the predicted spectra differ according to the high-energy particle physics model. In the Standard Evaporation Model (SEM) which incorporates the Standard Model of particle physics, a BH should directly Hawking-radiate the fundamental Standard Model particles whose de Broglie wavelengths are of the order of the black hole size [14]. Once the energy of the radiation approaches the Quantum Chromodynamics (QCD) confinement scale ($\sim 200 - 300$ MeV), quarks and gluons will be directly emitted [14]. As they stream away from the BH, the quarks and gluons should fragment and hadronize (analogous to jets seen in high-energy collisions in terrestrial accelerators) into the particles which are stable on astrophysical timescales [3]. Thus in the SEM, the evaporating black hole is an astronomical burst of photons, neutrinos, electrons, positrons, protons and anti-protons (and for sufficiently nearby sources, neutrons and anti-neutrons [15]).

The purpose of this paper is to examine the observational characteristics of the final evaporation phase of a BH according to the SEM, incorporating the recent LHC results for TeV energies, and to explore observational strategies that can be used in direct PBH burst searches, with particular relevance for the High Altitude Water Cherenkov (HAWC) observatory. Included is a discussion of the limitations and advantages of specific burst search methods and unique PBH burst signatures. In Section 2, we review the black hole Hawking radiation process and use an empirical fragmentation function to calculate the BH photon spectrum and light curve and to parameterize the instantaneous photon emission from a BH burst. In Section 3, we explore methods for direct searches for PBH bursts and the procedures for setting upper limits on the PBH distribution which would arise from null detection. In Section 4 we discuss how one can potentially differentiate a PBH burst from other known cosmological GRB sources. In Section 5, we discuss the applicability and limitations of various assumptions employed in our PBH burst properties calculations. A summary of our findings and conclusions is given in Section 6.

2. Photons from a PBH Burst

2.1. Hawking Radiation

Hawking showed that a black hole radiates each fundamental particle species at an emission rate of [2; 16]

$$\frac{d^2 N}{dE dt} = \frac{\Gamma/2\pi\hbar}{e^x - (-1)^{2s}} n_{\text{dof}}, \quad (1)$$

where s is the particle spin, n_{dof} is the number of degrees of freedom of the particle species (e.g. spin, electric charge, flavor and color), Γ is the absorption coefficient, and \hbar is the reduced Planck constant. The dimensionless quantity x is defined by

$$x \equiv \frac{8\pi G M_{BH} E}{\hbar c^3} = \frac{E}{k T_{BH}} \quad (2)$$

for a nonrotating, uncharged black hole, where E is the energy of the Hawking-radiated particle, M_{BH} is the black hole mass, T_{BH} is the black hole temperature,

$$k T_{BH} = \frac{\hbar c^3}{8\pi G M_{BH}} = 1.058 \left(\frac{10^{10} \text{ kg}}{M_{BH}} \right) \text{ GeV}, \quad (3)$$

G is the universal gravitational constant, c is the speed of light and k is Boltzmann's constant. Because initial black hole rotation and/or electric charge is radiated away faster than mass, we will assume a nonrotating, uncharged black hole in our analysis; extension to rotating and/or charged black holes is straightforward [14; 17; 18].

The absorption coefficient Γ depends on M_{BH} , E and s . For an emitted species of rest mass m , Γ at $E \gg mc^2$ has the form

$$\Gamma(M_{BH}, E, s) = 27 \left(\frac{x}{8\pi} \right)^2 \gamma_s(x) \quad (4)$$

such that $\gamma_s(x) \rightarrow 1$ for large x . The functions $\gamma_s(x)$ are shown in Figure 1 for massless or relativistic uncharged particles with $s = 0$, $s = 1/2$ and $s = 1$ [14; 19; 17; 18; 20; 21; 22]. For a non-relativistic $s = 1/2$ particle, Γ at $E = mc^2$ remains at least 50% of the relativistic value and, when $k T_{BH} \gtrsim 0.1 mc^2$, only deviates noticeably from the relativistic value at $E \lesssim 2 mc^2$ [18]. Below $E = mc^2$, $\Gamma = 0$. Electrostatic effects associated with the emission of a particle of electric charge e decrease Γ by at most a few percent [18].

Combining the above equations, the emission rate per fundamental particle species can be written in the form

$$\frac{d^2 N}{dE dt} = \frac{27}{2\pi\hbar(8\pi)^2} n_{\text{dof}} \psi_s(x) \quad (5)$$

where

$$\psi_s(x) \equiv \frac{\gamma_s(x)x^2}{e^x - (-1)^{2s}}. \quad (6)$$

The dimensionless emission rate functions, $\psi_s(x)$, are plotted in Figure 2 for $s = 0, 1/2$, and 1 . The distribution $\psi_s(x)$ peaks at $x = x_{r,s}$ where $x_{r,s=0} = 2.19$ for uncharged massless or relativistic $s = 0$ particles, $x_{r,s=1/2} = 4.02$ for relativistic $s = 1/2$ particles with charge $\pm e$, and $x_{r,s=1} = 5.77$ for uncharged massless or relativistic $s = 1$ particles [14; 19; 18; 20; 21; 22]. The emission rate integrated over energy, per emitted fundamental species, is

$$\frac{dN}{dt} = \int_0^\infty \frac{d^2 N}{dE dt} dE \quad (7)$$

$$= \frac{27c^3}{2\pi G(8\pi)^3 M_{BH}} n_{\text{dof}} \Psi_s = \frac{1.093 \times 10^{22}}{(M_{BH}/10^{10} \text{ kg})} n_{\text{dof}} \Psi_s \text{ s}^{-1} \quad (8)$$

$$= \frac{27kT_{BH}}{2\pi\hbar(8\pi)^2} n_{\text{dof}} \Psi_s = 1.033 \times 10^{22} \left(\frac{T_{BH}}{\text{GeV}} \right) n_{\text{dof}} \Psi_s \text{ s}^{-1} \quad (9)$$

where

$$\Psi_s \equiv \int_0^\infty \frac{\gamma_s(x)x^2}{e^x - (-1)^{2s}} dx. \quad (10)$$

Per degree of freedom, $\Psi_{s=0} = 2.45$ for uncharged massless or relativistic $s = 0$ particles, $\Psi_{s=1/2} = 0.897$ for uncharged relativistic $s = 1/2$ particles, $\Psi_{s=1/2} = 0.879$ for relativistic $s = 1/2$ particles with charge $\pm e$, and $\Psi_{s=1} = 0.273$ for uncharged massless or relativistic $s = 1$ particles [14; 19; 18; 20; 21; 22].

Figure 3 displays the direct radiation rates according to Equation 1 for a single relativistic quark flavor ($n_{\text{dof}} = 12$) and for gluons ($n_{\text{dof}} = 16$), as functions of x . (In Figure 3 we have neglected the electric charge of the quark which affects the quark emission rate by less than 5 percent [14; 18].)

In order to calculate the spectrum of the final photon burst from the PBH, two important relations pertaining to the final phase of BH evaporation are

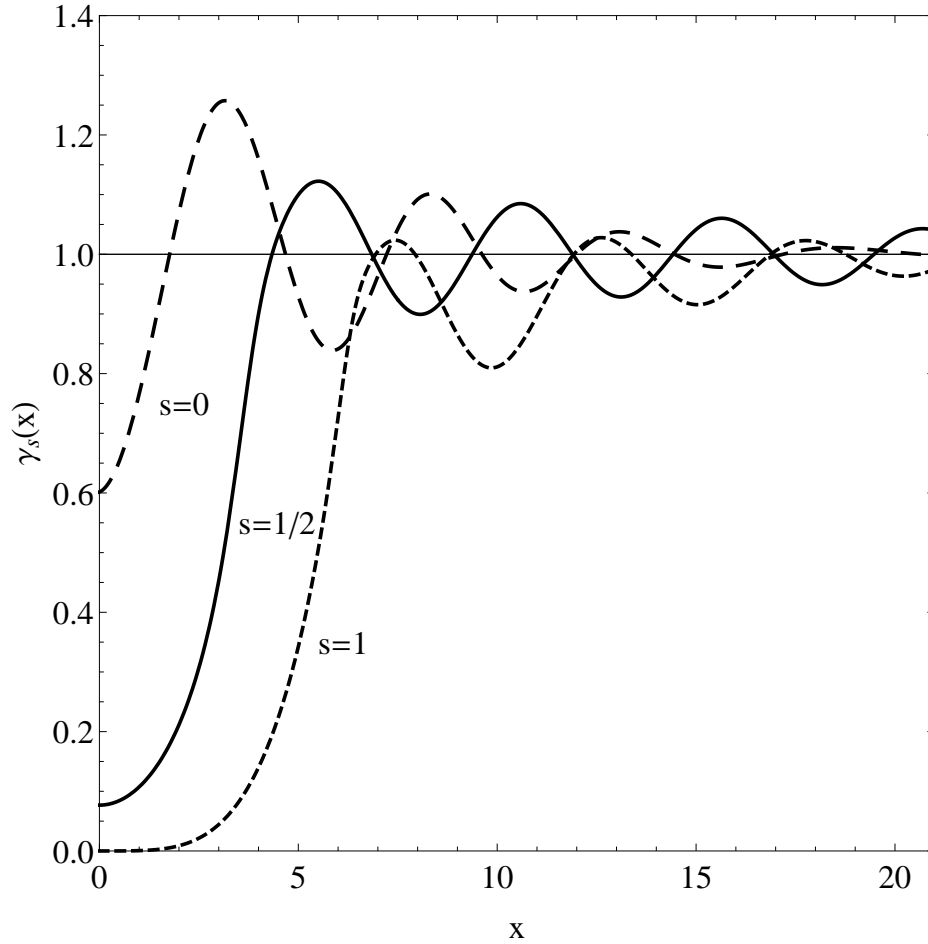


Figure 1: The functions $\gamma_s(x)$ for massless spin-0 (long dashed line), spin-1/2 (solid line) and spin-1 (short dashed line) particles.

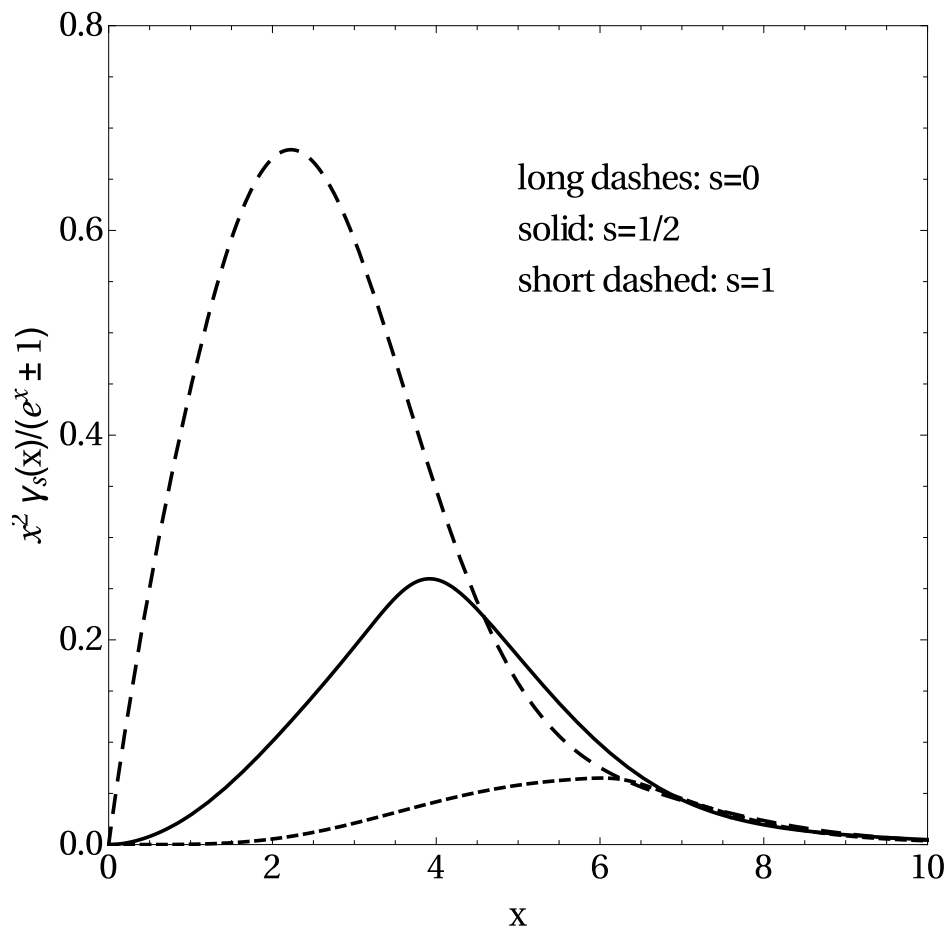


Figure 2: The dimensionless emission rate per degree of freedom, $\psi_s(x) = x^2\gamma(x)/(e^x \pm 1)$ as a function of x for $s = 0, 1/2$, and 1 .

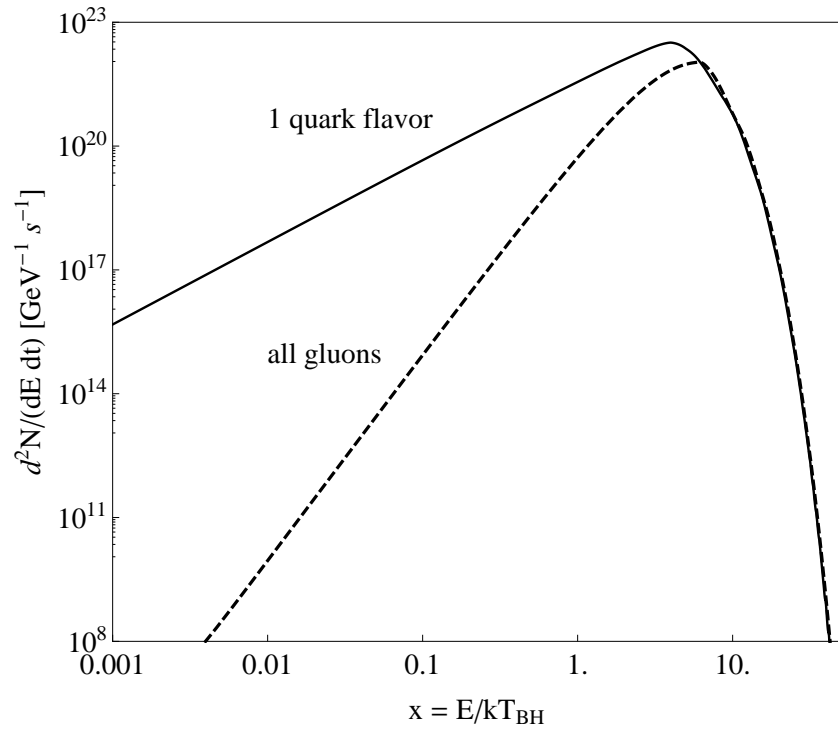


Figure 3: Rates of Hawking radiation of a massless quark flavor and of gluons, as functions of x . For $x \ll 1$, the power laws are $\psi \propto x^2$ for $s = 1/2$ and $\psi \propto x^3$ for $s = 1$.

needed. The first relation we require is the black hole mass M_{BH} as a function of time [19]

$$\frac{dM_{BH}}{dt} \equiv -\frac{\alpha(M_{BH})}{M_{BH}^2}, \quad (11)$$

where the function $\alpha(M_{BH})$ incorporates all directly emitted particle species and their degrees of freedom. As the BH evaporates, the value of M_{BH} is reduced by an amount equal to the total mass-energy of the emitted particles. By conservation of energy,

$$\frac{d(M_{BH}c^2)}{dt} = -\sum_i \int_0^\infty \frac{d^2 N_i}{dE dt} E dE \quad (12)$$

where the summation over i is over all the fundamental species and so

$$\alpha(M_{BH}) = \frac{M_{BH}^2}{c^2} \sum_i \int_0^\infty \frac{d^2 N_i}{dE dt} E dE. \quad (13)$$

Substituting for M_{BH} in terms of T_{BH} and E in terms of x , we can write

$$\alpha(M_{BH}) = \frac{27\hbar c^4}{2\pi G^2 (8\pi)^4} \sum_i \int_0^\infty n_{\text{dof},i} \phi_{s_i}(x) dx \quad (14)$$

where $\phi_s(x) \equiv \psi_s(x)x$.

The dimensionless emitted power functions, $\psi_s(x)$, are shown in Figure 4 for $s = 0, 1/2$, and 1 . The distribution $\phi_s(x)$, and hence the instantaneous power emitted in each fundamental state, peaks at $x = x_{p,s}$ where $x_{p,s=0} = 2.66$ for uncharged massless or relativistic $s = 0$ particles, $x_{p,s=1/2} = 4.40$ for uncharged relativistic $s = 1/2$ particles, $x_{p,s=1/2} = 4.53$ for relativistic $s = 1/2$ particles with charge $\pm e$, and $x_{p,s=1} = 6.04$ uncharged massless or relativistic $s = 1$ particles [14; 19; 18; 20; 21; 22]. As the remaining BH evaporation lifetime τ decreases, T_{BH} increases and new fundamental quanta begin to contribute significantly to $\alpha(M_{BH})$ once T_{BH} crosses each relevant mass threshold, $kT_{BH} \sim m_i c^2 / x_{p,s_i}$. At $kT_{BH} \gtrsim m_i c^2$, the contribution of a specific fundamental species i to $\alpha(M_{BH})$ is

$$\alpha_i = \frac{27\hbar c^4}{2\pi G^2 (8\pi)^4} n_{\text{dof},i} \Phi_{s_i} = 2.06 \times 10^{15} n_{\text{dof},i} \Phi_{s_i} \text{ kg}^3 \text{ s}^{-1}, \quad (15)$$

where

$$\Phi_s = \int_0^\infty \frac{\gamma_s(x)x^3}{e^x - (-1)^{2s}} dx. \quad (16)$$

Per degree of freedom, $\Phi_{s=0} = 6.89$ for massless or relativistic $s = 0$ particles, $\Phi_{s=1/2} = 3.79$ for uncharged relativistic $s = 1/2$ particles, $\Phi_{s=1/2} = 3.68$ for relativistic $s = 1/2$ particles with charge $\pm e$, and $\Phi_{s=1} = 1.56$ for massless or relativistic $s = 1$ particles [14; 19; 18; 20; 21; 22]. From the values for uncharged and $\pm e$ -charged $s = 1/2$ modes, we can linearly interpolate approximate values for relativistic $\pm e/3$ -charged d , s and b quarks, $\Phi_{s=1/2} \simeq 3.75$ per degree of freedom, and for relativistic $\pm 2e/3$ -charged u , c and t quarks, $\Phi_{s=1/2} \simeq 3.72$ per degree of freedom.

Counting only the experimentally confirmed fundamental Standard Model particles [23], a $kT_{BH} \simeq 1$ GeV ($M_{BH} \simeq 10^{10}$ kg) black hole should directly emit the following field quanta: the three charged leptons ($s = 1/2$, $n_{dof} = 12$); the three neutrinos ($s = 1/2$, $n_{dof} = 6$) where we assume that the neutrinos are Majorana particles with negligible mass; five quark flavors ($s = 1/2$, $n_{dof} = 60$); the photon ($s = 1$, $n_{dof} = 2$); and the gluons ($s = 1$, $n_{dof} = 16$). This gives

$$\alpha(kT_{BH} \simeq 1 \text{ GeV}) = 6.6 \times 10^{17} \text{ kg}^3\text{s}^{-1}. \quad (17)$$

At $kT_{BH} \simeq 50$ GeV ($M_{BH} \simeq 2 \times 10^8$ kg), the list also includes the top quark, the W^\pm and Z^0 massive vector bosons ($s = 1$, $n_{dof} = 9$), and the Higgs boson ($s = 0$, $n_{dof} = 1$, and treating the Higgs boson as a 125 GeV resonance [24]). This gives

$$\alpha(kT_{BH} \simeq 50 \text{ GeV}) = 8.0 \times 10^{17} \text{ kg}^3\text{s}^{-1}. \quad (18)$$

Energies well above the Higgs field vacuum expectation value ~ 246 GeV have not yet been explored in high energy accelerators. The ten fundamental modes of W^\pm , Z^0 and H^0 are expected to be counted differently above the electroweak symmetry breaking phase transition because of expected restoration of $SU(2) \times U(1)$ gauge symmetry [25], although this has yet to be confirmed in accelerator experiments. By the Goldstone Boson Equivalence Theorem, the longitudinal modes of the W^\pm and Z^0 bosons observed at lower energies are expected to be expressed as scalar modes at these energies. In this case, there would be 6 transverse vector $s = 1$ fields and 4 scalar $s = 0$ fields of W^\pm , Z^0 and H^0 , giving an the asymptotic value of $\alpha(M_{BH}) \simeq 8.3 \times 10^{17} \text{ kg}^3\text{s}^{-1}$ for $kT_{BH} > 100$ GeV ($M_{BH} < 10^8$ kg). Because this has not yet been observed experimentally and there are other possible arrangements at high energies, however, we will confine our modes to those

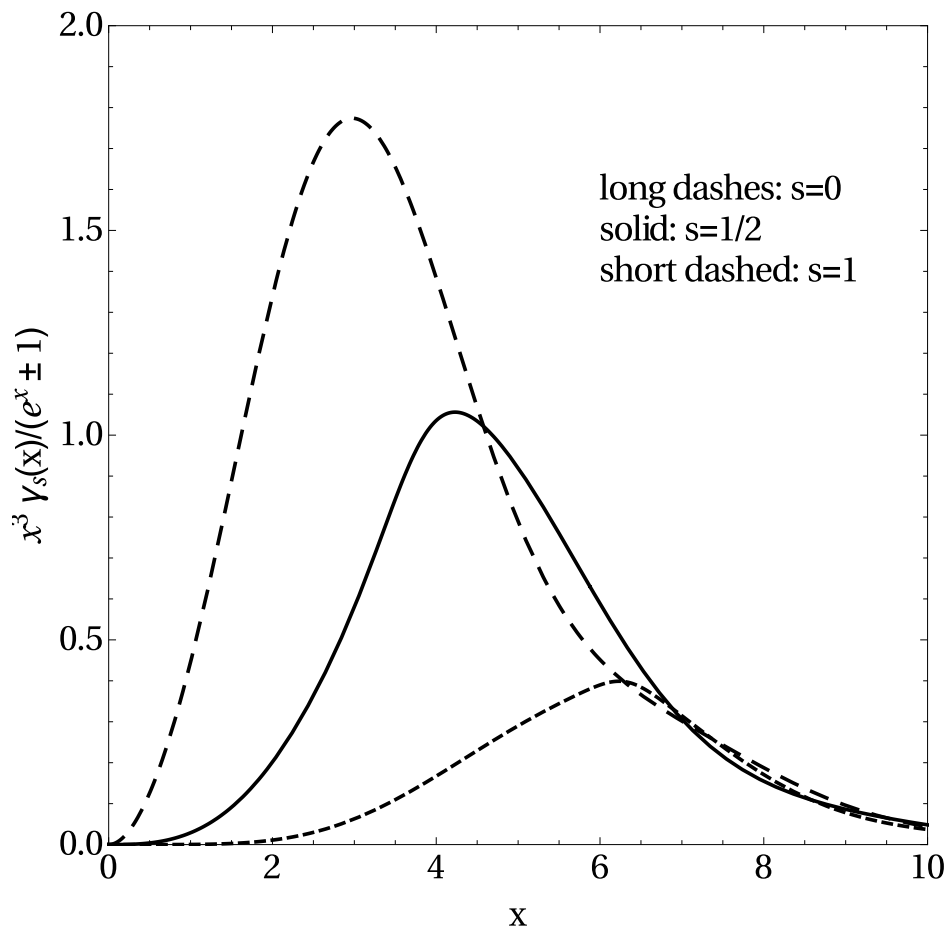


Figure 4: The dimensionless emitted power per degree of freedom, $\phi_s(x) = x^3 \gamma(x)/(e^x \pm 1)$ as a function of x for $s = 0, 1/2$, and 1 .

which have been experimentally confirmed and use as our asymptotic value of $\alpha(M_{BH})$ in subsequent calculations

$$\alpha_{SM} = 8.0 \times 10^{17} \text{kg}^3 \text{s}^{-1} \quad (19)$$

for $kT_{BH} > 100 \text{ GeV}$ ($M_{BH} < 10^8 \text{ kg}$). We note that the ambiguity in counting $s = 0$ and $s = 1$ states as T_{BH} transitions through and above the electroweak symmetry breaking scale has a negligible effect on the BH emission spectra because of the dominance of the $s = 1/2$ modes at these T_{BH} .

Figure 5 illustrates $\alpha(M_{BH})$ and $\alpha(T_{BH})$ for the SEM. In Figure 5, the function is presented as piece-wise constant with each horizontal line segment representing the sum of the asymptotic contributions for $kT_{BH} > m_i c^2 / x_{p,si}$. As the end of the BH's lifetime approaches, T_{BH} exceeds the rest masses of all known fundamental particles, and α reaches a constant asymptotic value, α_{SM} .

For the current and future generations of very high energy (VHE) gamma-ray observatories, we are interested in bursts generated by black holes of temperature $kT_{BH} \gtrsim 1 \text{ TeV}$. For $kT_{BH} \gtrsim 1 \text{ TeV}$ (corresponding to $M_{BH} \lesssim 10^7 \text{ kg}$ and a remaining evaporation lifetime of $\tau \lesssim 500 \text{ s}$), we have

$$\alpha(kT_{BH} \gtrsim 1 \text{ TeV}) \approx \alpha_{SM} = 8.0 \times 10^{17} \text{kg}^3 \text{s}^{-1}. \quad (20)$$

Returning to Equation 11, the BH mass as a function of remaining evaporation lifetime τ in this regime is then

$$M_{BH}(\tau) \approx (3\alpha_{SM} \tau)^{1/3} = 1.3 \times 10^6 \left(\frac{\tau}{1\text{s}} \right)^{1/3} \text{kg}. \quad (21)$$

The second relation we require is the BH temperature T_{BH} expressed as a function of τ for the final evaporation phase. Combining Equations 3 and 21, we have for $kT_{BH} \gtrsim 1 \text{ TeV}$

$$kT_{BH} = 7.8 \left(\frac{\tau}{1\text{s}} \right)^{-1/3} \text{TeV} \quad (22)$$

$$\tau = 4.8 \times 10^2 \left(\frac{kT_{BH}}{\text{TeV}} \right)^{-3} \text{s}. \quad (23)$$

Strictly, the above equations apply provided that the black hole temperature is below the Planck temperature T_{Pl} ($\simeq 1.22 \times 10^{16} \text{ TeV}$). However,

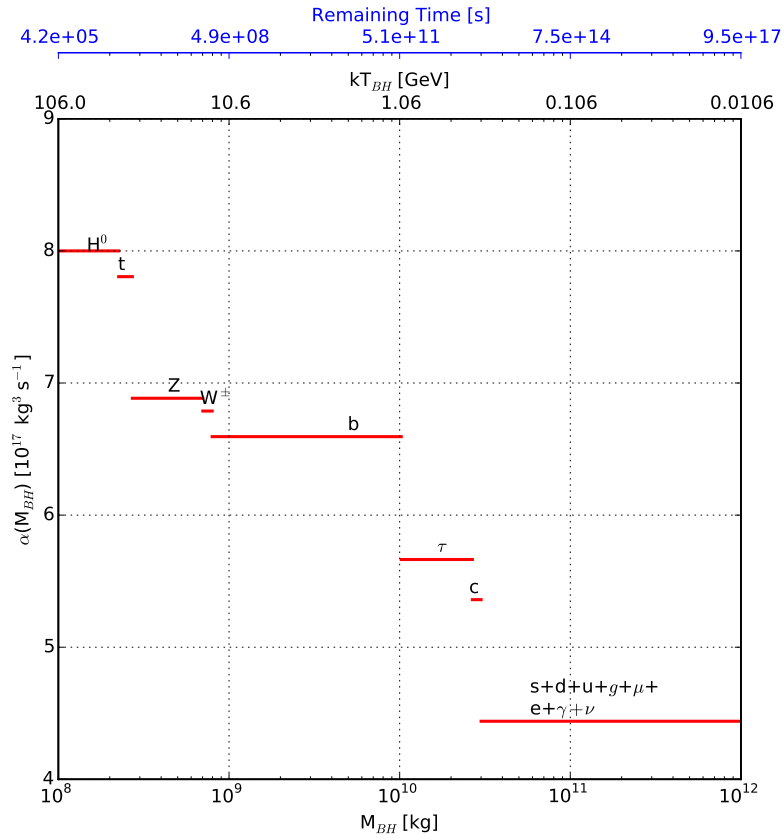


Figure 5: The function $\alpha(M_{BH})$ in the Standard Evaporation Model. The asymptotic value for the SEM is $8.0 \times 10^{17} \text{ kg}^3 \text{ s}^{-1}$.

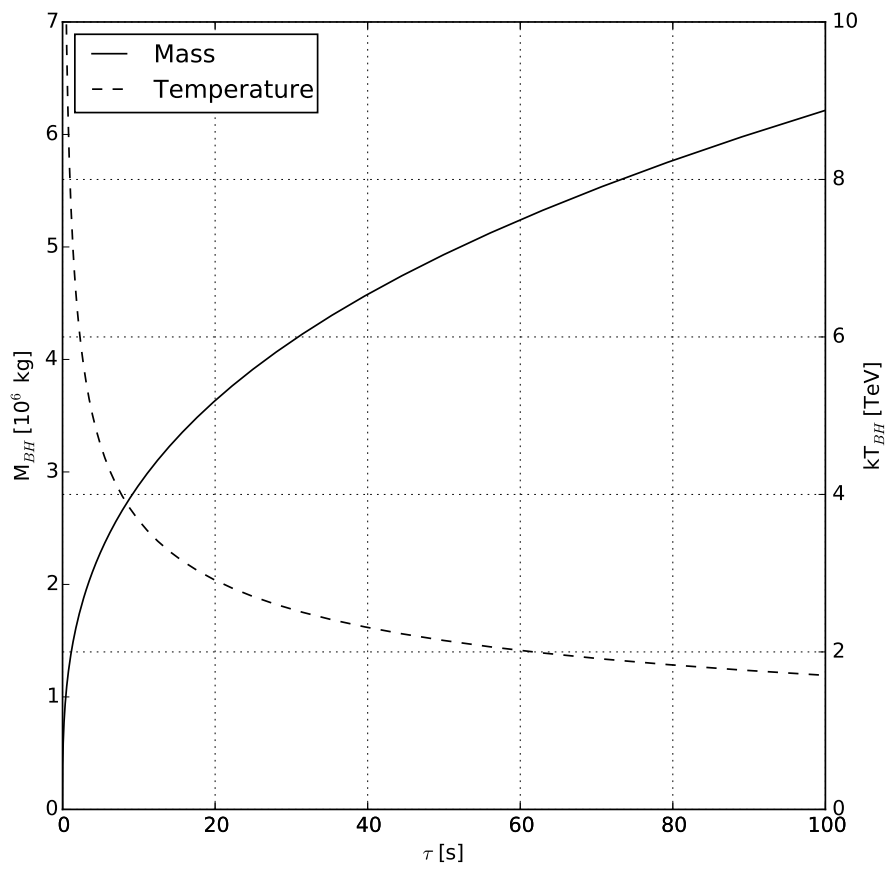


Figure 6: Black hole mass and temperature for the final 100 seconds of the BH evaporation lifetime (τ is the remaining time). The decrease of mass and the increase of temperature accelerate as $\tau \rightarrow 0$.

because the remaining evaporation lifetime dramatically shortens as T_{BH} increases, the behavior of the BH close to T_{P1} has negligible effect on the astronomically observable emission spectra.

The black hole mass and temperature for the final 100 s of evaporation lifetime, corresponding to temperatures $kT_{BH} \gtrsim 2$ TeV, are shown in Figure 6. VHE gamma-ray observatories are sensitive to photon energies in the range from ~ 50 GeV to 100 TeV. Thus the relevant x range for the final 100 s of the PBH burst is $0 \lesssim x \lesssim 50$. The instantaneous emission rates for a relativistic quark flavor and for gluons as a function of x in this range is included in Figure 3.

In order to elucidate the behaviour near the end of the black hole's evaporation lifetime, we now investigate the emission rate and spectrum as functions of τ . Figure 7 shows the instantaneous emission rate $d^2N/(dEdt)$ for a relativistic or massless quark flavor, as a function of quark energy E , when $\tau = 100, 10, 1, 0.1, 0.01$ and 0.001 s. As $\tau \rightarrow 0$ and T_{BH} increases, the emission rate per directly Hawking-radiated $s = 1/2$ degree of freedom is constant at the peak but increases at high energies and decreases at low energies because the location of the peak scales with T_{BH} .

The SEM theory of Hawking radiation in the final 100 seconds has only one parameter with physical dimensions, which may be taken to be kT_{BH} . Because $kT_{BH} \gtrsim 2$ TeV is much larger than any Standard Model particle rest mass, all Hawking-radiated particles may be approximated as ultra-relativistic. Thus the $kT_{BH} \gtrsim 2$ TeV instantaneous emission rate per fundamental particle species depends essentially only on the ratio $x = E/kT_{BH}$, as in Figure 3: the dependence of the rate on E is the same for different τ values except for a translation proportional to T_{BH} (see Figure 7) and the SEM Hawking radiation rate per degree of freedom has a scale invariance with respect to x .

This scale invariance leads to useful power law approximations. For example, the direct Hawking emission rate for Dirac particles with $x \ll 1$ is proportional to x^2 (recall Figure 3) and the direct Hawking emission rate for vector $s = 1$ particles with $x \ll 1$ is proportional to x^3 [19]. Other power laws appear in the emission rate for the final state photons that are created in the decays of the directly Hawking-radiated quarks and gluons.

2.2. QCD Fragmentation

According to the SEM, Equation 1 applies to the direct Hawking radiation of the fundamental particles of the Standard Model of high-energy

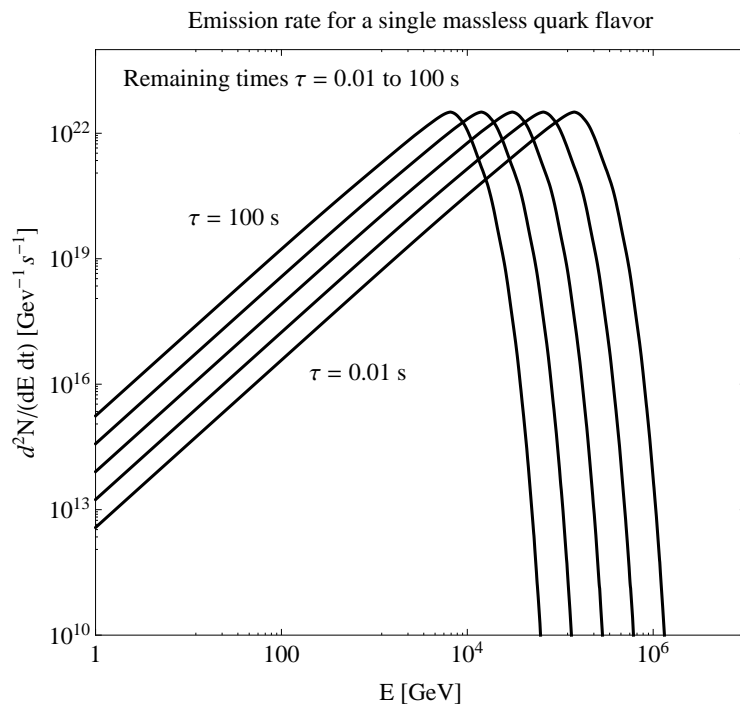


Figure 7: Instantaneous number emission rate for a single massless quark flavor, as a function of quark energy E , at five values of remaining evaporation lifetime τ : 100, 10, 1, 0.1, 0.01 seconds.

physics: the leptons, quarks, and the gauge bosons [2; 16; 19; 26; 14]. As they stream away from the BH, these fundamental particles will then evolve by Standard Model processes, ultimately into the particles which are stable on astrophysical timescales: photons, neutrinos, electrons, positrons, protons and anti-protons (and for sufficiently nearby sources, neutrons and anti-neutrons³). In particular, quarks and gluons will undergo fragmentation and hadronization into intermediate states which will eventually decay into the astrophysically stable particles.

For application to PBH searches at VHE gamma-ray observatories, we seek the total photon emission rate from the BH. The photon production has several components⁴: (i) The “direct photons” produced by the direct Hawking radiation of photons: this component peaks at a few times T_{BH} and is most important at the highest photon energies at any given T_{BH} . (ii) The “fragmentation photons” arising from the fragmentation and hadronization of the quarks and gluons which are directly Hawking-radiated by the BH (in particular, quark and gluon fragmentation and hadronization generates π^0 's which decay into 2 photons with a branching fraction of 98.8%): this component is the dominant source of photons at energies below T_{BH} . (iii) The photons produced by the decays of other Hawking-radiated fundamental particles, e.g., the tau lepton, W and Z gauge bosons, and Higgs boson; this component is small compared to the component produced by the fragmentation of directly Hawking-radiated quarks and gluons and is neglected here. (We note that because the W , Z , and Higgs bosons decay predominantly via hadronic channels, their main effect is to enhance the fragmentation photon component by at most $\sim 10\%$.)

In the SEM, the production rate of hadrons by the BH is equal to the integrated convolution of the Hawking emission rates for the relevant fundamental particles i (Equation 1) with fragmentation functions $D_{h/i}(z)$ describing the fragmentation of species i into hadron h , where $z = E_h/E$ is the

³Because the mean lifetime of a neutron at rest is $\sim 10^3$ s, undecayed neutrons of high energy E_N should arrive from PBHs closer than $\sim (E_N/100 \text{ TeV}) \text{ pc}$.

⁴ Because we are investigating photon energies $\gtrsim 50 \text{ GeV}$, we do not include the white inner bremsstrahlung photon component generated by the Hawking radiation of charged fermions which is dominated at these energies by the fragmentation photons [27].

fraction of the initial particle's energy E carried by the hadron; i.e.,

$$\frac{d^2 N_h}{dE_h dt} = \sum_i \int_{m_h c^2}^{\infty} \int_0^1 \frac{d^2 N_i}{dE dt} D_{h/i}(z) \delta(E_h - zE) dz dE. \quad (24)$$

Here the summation is over all contributing fundamental species i and $D_{h/i}(z)dz$ is the number of hadrons h with energy fraction in the range from z to $z+dz$ produced by the fragmentation of fundamental particle i .

For the current study, we wish to describe the photon burst generated in the final moments of the BH's evaporation lifetime and the resulting light curve and energy spectrum seen by the detector. Fragmentation functions $D_{b/a}(z)$ have been measured in high-energy physics experiments, such as e^+e^- annihilation, for a variety of initial partons (a) and final fragments (b) [28; 29]. However, a complete set of fragmentation functions is not available. We turn therefore to a simplified fragmentation model. This model, which has appeared in the literature previously to estimate the photons derived from the fragmentation of partons [30; 31; 4], is expected to provide a realistic representation of the photon spectrum for our purpose and has been used in the analyses of PBH searches by several gamma-ray observatories [7; 9]. Alternatively, Equation 24 can be evaluated using a Monte Carlo simulation which incorporates a parton showering program such as Pythia [32] or Herwig [33] extended to generate decays into the astrophysically stable species, including photons. This approach has also previously been used in PBH flux calculations [14] and is necessary if the goal is to obtain full spectral details about the instantaneous flux of final-state particle species. We note that in both approaches, the $kT_{BH} \gtrsim 2$ TeV BH burst calculation requires extrapolation of the fragmentation functions or event generator codes to higher energies than have been validated in accelerator experiments.

2.3. The Pion Fragmentation Model

For photon production, the most important decay from the fragmentation of the initial quark or gluon is $\pi^0 \rightarrow 2\gamma$. In the pion fragmentation model, we proceed assuming that the QCD fragmentation of quarks and gluons may be approximated entirely by the production of pions. Two questions must be addressed by the model: what is the pion spectrum generated by the partons and what is the photon spectrum generated by the pion decays?

To answer the first question, we utilize a heuristic fragmentation function

$$D_{\pi/i}(z) = \frac{15}{16} z^{-3/2} (1-z)^2 \quad (25)$$

where $z \equiv E_\pi/E$ is the energy fraction carried by a pion generated by a parton of energy E [4; 30; 31]. This function is normalized such that $\int_0^1 z D_{\pi/i}(z) dz = 1$; i.e., all of the initial parton energy is converted to go into pions. Figure 8 shows the fragmentation function $D_{\pi/i}(z)$. The results in this paper are based on assuming the pion fragmentation function $D_{\pi/i}(z)$ of Equation 25 for all initial Hawking-radiated quarks and gluons. We note, though, that the function Equation 25 implies an average energy for the final state photons and a multiplicity (number) of final state photons per initial parton which match the $T_{BH}^{1/2}$ scaling of the photon average energy and multiplicity found using a HERWIG-based Monte Carlo simulation to generate fragmentation and hadronization of the Hawking-radiated particles from $1 \text{ GeV} \leq T_{BH} \leq 100 \text{ GeV}$ black holes [14]. We discuss the accuracy of this heuristic model further in Section 5.1.⁵

The instantaneous pion production rate by the BH is then

$$\frac{d^2 N_\pi}{dE_\pi dt} = \sum_i \int_{m_\pi c^2}^\infty \int_0^1 \frac{d^2 N_i}{dE_i dt} D_{\pi/i}(z') \delta(E_\pi - z' E_i) dz' dE_i. \quad (26)$$

Figure 9 shows the instantaneous pion rate as a function of $x_\pi \equiv E_\pi/kT_{BH}$. At high pion energies, the pion rest mass is negligible and this function has a scaling form: it depends only on the dimensionless ratio x_π . (Similarly, we saw that the quark and gluon rates depend only on $x = E/kT_{BH}$ when T_{BH} is large compared to the quark masses.) Comparing Figures 3 and 9 elucidates how the fragmentation of quarks and gluons at high energies, say $E > 10 - 100 \text{ TeV}$, yields a significant flux of pions at lower energies, say $1 \text{ GeV} < E_\pi < 100 \text{ TeV}$; the π^0 decays then produce photons in the detectable energy range of VHE gamma-ray observatories.

We assume that the pions are generated by the fragmentation and hadronization of the 72 directly Hawking-radiated $s = 1/2$ quark modes and the 16 directly Hawking-radiated $s = 1$ gluon modes. The directly Hawking-radiated W^\pm and Z^0 bosons also decay via hadronic jets about 70% of the time. Because W^\pm and Z^0 are expected to each have only two polarization states when $kT_{BH} \gtrsim 1 \text{ TeV}$ (giving a total of 6 fundamental degrees of freedom)

⁵ The function $D_{\pi/i}(z)$ resembles closely the result of a QCD calculation [30] which has been used for theoretical calculations in a previous PBH search [9]. Section 5.1 has a discussion of the heuristic fragmentation function $D_{\pi/i}(z)$, compared to empirical fragmentation functions that have been extracted from collider data.

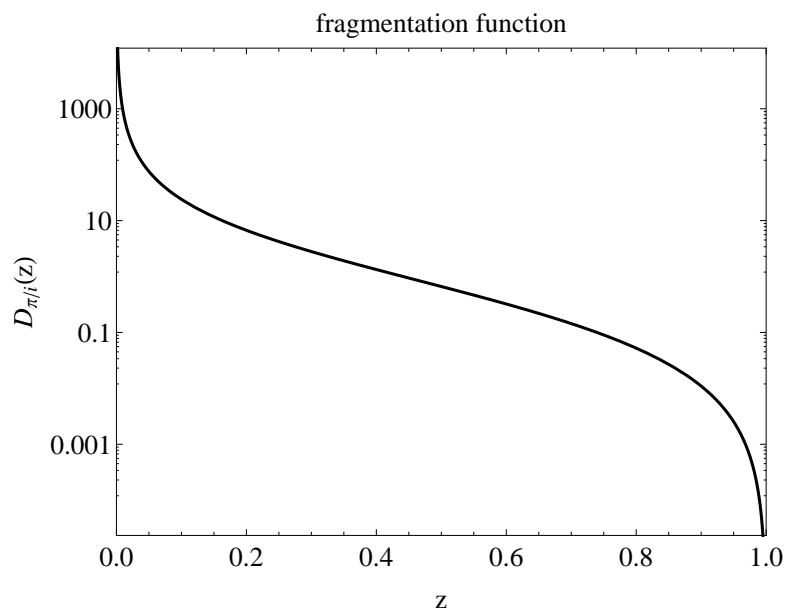


Figure 8: The heuristic fragmentation function $D_{\pi/i}(z)$ as a function of the pion energy fraction, z .

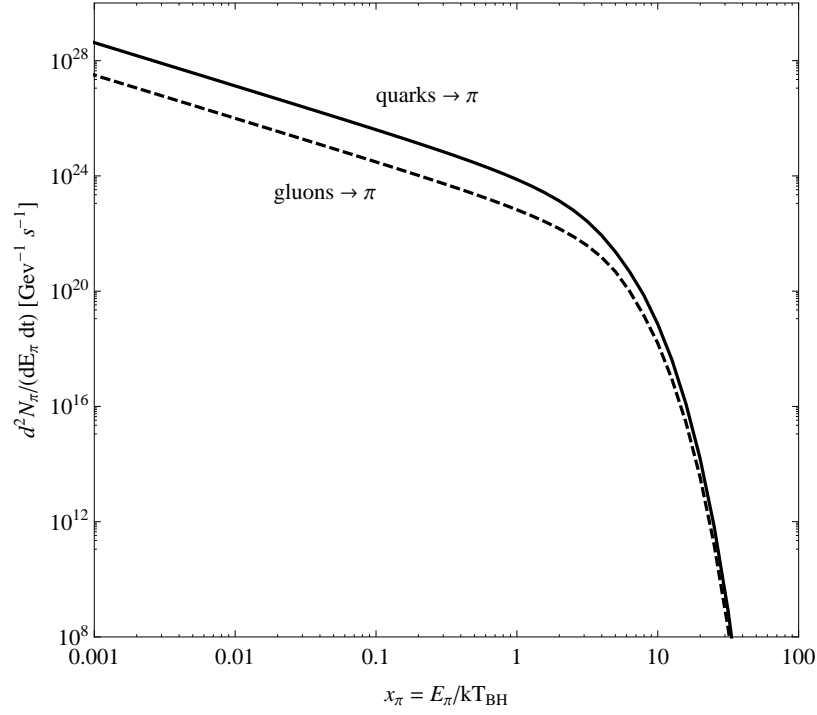


Figure 9: The pion production rate $d^2 N_\pi / (dE_\pi dt)$ calculated from Equation 26, plotted as a function of $x_\pi = E_\pi / kT_{BH}$. The number of degrees of freedom is $n_{\text{dof}} = 72$ for quarks and $n_{\text{dof}} = 16$ for gluons. The quark contribution is dominant. For $x_\pi < 1$ the particle rate obeys a power law: $d^2 N_\pi / (dE_\pi dt) \propto x_\pi^{-3/2}$. The power index of $-3/2$ matches the low- z behaviour of the assumed fragmentation function, which varies as $z^{-3/2}$.

and $\Psi_{s=1/2} \simeq 3\Psi_{s=1}$, however, the Hawking-radiated W^\pm and Z^0 increase the instantaneous pion production rate of Figure 7 by only $\sim 3\%$.

Higgs modes also contribute to the pion flux to a small extent. The dominant decay modes for the experimentally-confirmed H^0 resonance at 125 GeV are $H^0 \rightarrow b + \bar{b}$ and $H^0 \rightarrow W^+ + W^-$. The dominant decay modes of any other Higgs states (which have not yet been discovered) are also expected to be $H \rightarrow q + \bar{q}$ and decays via W^\pm and Z^0 bosons. Noting that $\Psi_{s=0} \simeq 2\Psi_{s=1/2}$, the directly Hawking-radiated Higgs boson states can increase the instantaneous pion production rate of Figure 9 by at most $\sim 10\%$.

2.4. Photon Flux from Pion Fragmentation

We now obtain the photon flux from the $\pi^0 \rightarrow 2\gamma$ decay of the pion distribution. Because the fragmentation function $D_{\pi/i}(z)$ includes all three pion charge states π^+ , π^- , and π^0 as equal components⁶, and each π^0 decays into two photons, we must multiply by 2/3 to get the γ multiplicity. In the π^0 rest frame, the two photons have equal but opposite momenta and equal energies, $m_\pi c^2/2$. In the reference frame of the gamma-ray observatory detector, the energies of the two photons, E_γ , are unequal but complementary fractions of the π^0 energy in the detector frame, E_π . We assume that only one of the photons in each pair is detectable.⁷

Let θ be the angle between the momentum of the observed photon in the π^0 rest frame and the π^0 momentum in the detector frame. In the detector frame, $E_\gamma = (E_\pi/2)(1 + \beta \cos \theta)$ where the π^0 velocity $\beta = v/c \approx 1$ and $E_\pi = m_\pi/\sqrt{1 - \beta^2}$. Because the angular distribution of the photons is isotropic in the π^0 rest frame, the distribution of pion-produced photons in the detector frame is

$$\left(\frac{d^2 N_\gamma}{dE_\gamma dt}\right)_{\text{frag.}} = \frac{2}{3} \int_{-1}^1 \frac{2\pi d \cos \theta}{4\pi} \int_{m_\pi}^\infty \frac{d^2 N_\pi}{dE_\pi dt} \delta[E_\gamma - (E_\pi/2)(1 + \beta \cos \theta)] dE_\pi. \quad (27)$$

⁶ The charged pions do not contribute to the photon flux. However, they do yield neutrinos. The same heuristic model can be used to estimate the flux of neutrinos from the BH.

⁷ The angle between the 2 photon trajectories in the detector frame will be very small because of the large Lorentz boost. However, if the BH is at a distance of order 1 parsec from the detector, then only one of the photons from each π^0 decay will hit the detector.

Evaluating the integral over $\cos\theta$, we have

$$\left(\frac{d^2 N_\gamma}{dE_\gamma dt}\right)_{\text{frag.}} = \frac{2}{3} \int_{E_{\min}}^{\infty} \frac{d^2 N_\pi}{dE_\pi dt} \frac{dE_\pi}{\sqrt{E_\pi^2 - m_\pi^2}}. \quad (28)$$

For $E_\gamma > m_\pi/4$, the minimum pion energy is $E_{\min} = E_\gamma + m_\pi^2/(4E_\gamma)$. Equation 28 implies that the photon energy in the detector frame is uniformly distributed in the range

$$\frac{E_\pi(1 - \beta)}{2} \leq E_\gamma \leq \frac{E_\pi(1 + \beta)}{2}. \quad (29)$$

For high energy photons, we may approximate $m_\pi \approx 0$. In this case, the pion fragmentation function of Equation 25 evolves into the photon distribution per initial parton

$$D_{\gamma/i}(z_\gamma) = \frac{15}{16} \left(\frac{16}{3} + \frac{2}{3} z_\gamma^{-3/2} - 4z_\gamma^{-1/2} - 2z_\gamma^{1/2} \right) \quad (30)$$

where $z_\gamma \equiv E_\gamma/E$ is the energy fraction carried by a photon generated by a parton of energy E .

Figure 10 shows the instantaneous photon spectrum, including the directly Hawking-radiated photons, emitted by the black hole when the remaining BH evaporation lifetime is $\tau = 100, 10, 1, 0.1$ and 0.01 s.

2.5. Parameterization of the Black Hole Photon Spectrum

2.5.1. New Parameterization of Photon Flux from a TeV Black Hole

To simplify subsequent calculations, we parameterize the function for the fragmentation component of the total photon emission rate from the BH as follows. This parameterization is valid for $E_\gamma \gtrsim 1$ GeV.

By the scale invariance at short remaining time τ , $d^2 N_\gamma/(dE_\gamma dt)$ depends on the ratio

$$x_\gamma = \frac{E_\gamma}{kT_{BH}(\tau)} = 1.287 \times 10^{-4} \left(\frac{E_\gamma}{1 \text{ GeV}} \right) \left(\frac{\tau}{1 \text{ s}} \right)^{1/3}. \quad (31)$$

Fitting the curve shown in Figure 10, we derive a reasonable parameterization of the fragmentation contribution to be

$$\left(\frac{d^2 N_\gamma}{dE_\gamma dt}\right)_{\text{frag.}} = Ax_\gamma^{-3/2} [1 - \Theta_S(x_\gamma - 0.3)] \quad (32)$$

$$+ B \exp(-x_\gamma) [x_\gamma(x_\gamma + 1)]^{-1} \Theta_S(x_\gamma - 0.3) \quad (33)$$

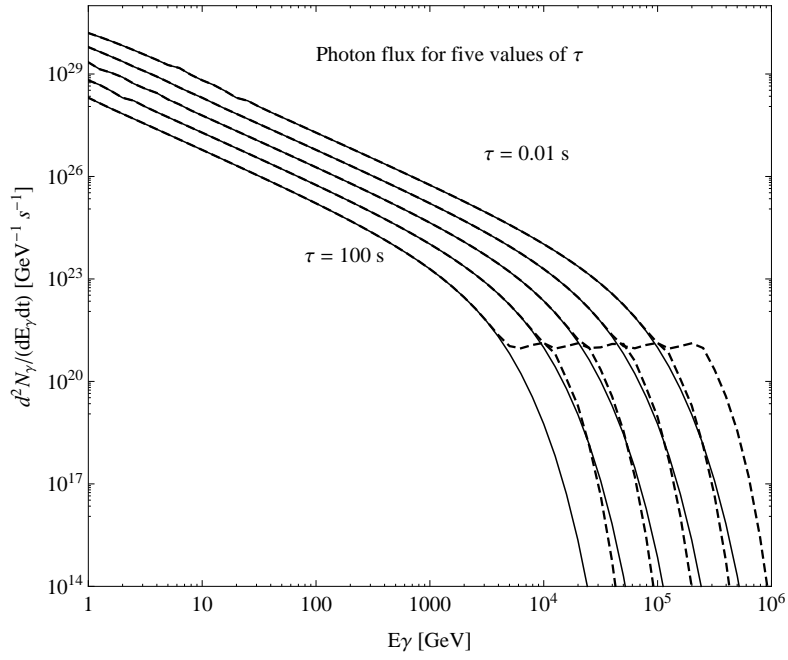


Figure 10: The instantaneous photon emission rate $d^2 N_\gamma / (dE_\gamma dt)$ for five values of the remaining burst lifetime, $\tau = 100, 10, 1, 0.1,$ and 0.01 s. The dashed curves show the total (fragmentation + direct) gamma-ray emission rate; the solid curves show the fragmentation only rate. As τ decreases, the rate increases.

where

$$A = 6.339 \times 10^{23} \text{GeV}^{-1} \text{s}^{-1}, \quad B = 1.1367 \times 10^{24} \text{GeV}^{-1} \text{s}^{-1} \quad (34)$$

and

$$\Theta_S(u) = 0.5(1 + \tanh(10u)). \quad (35)$$

The accuracy of this parameterization is $\pm 15\%$ for $0.1 \leq x_\gamma \leq 10$, and $\pm 3\%$ for smaller and larger x_γ . This is sufficient for most of our purposes. If greater accuracy is required, a table of the ratios of the approximate value to the exact value is used to correct the parameterized value.

We also derive, by curve-fitting, a parameterization of the directly Hawking-radiated photon component to be

$$\left(\frac{d^2 N_\gamma}{dE_\gamma dt} \right)_{\text{direct}} = \frac{(1.13 \times 10^{19} \text{GeV}^{-1} \text{s}^{-1})(x_\gamma)^6}{\exp(x_\gamma) - 1} F(x_\gamma) \quad (36)$$

where

$$F(x_\gamma) = 1.0 \quad \text{for } x_\gamma \leq 2 \quad (37)$$

and

$$F(x_\gamma) = \exp \{ [-0.0962 - 1.982 (\ln x_\gamma - 1.908)] \\ \times [1 + \tanh(20(\ln x_\gamma - 1.908))] \} \quad \text{for } x_\gamma > 2. \quad (38)$$

2.5.2. Comparison with Linton et al. Parameterization

A parameterization of the total photon emission rate by Linton et. al [9], which has often been used in PBH searches by high-energy observatories, is

$$\frac{d^2 N_\gamma}{dE_\gamma dt} = 6.24 \times 10^{23} \left[\frac{1}{8} \left(\frac{Q}{E_\gamma} \right)^{3/2} - \frac{3}{4} \sqrt{\frac{Q}{E_\gamma}} - \frac{3}{8} \sqrt{\frac{E_\gamma}{Q}} + 1 \right] \text{GeV}^{-1} \text{s}^{-1}, \quad \text{for } E_\gamma < Q \quad (39)$$

$$\frac{d^2 N_\gamma}{dE_\gamma dt} = 10^{21} \left(\frac{Q}{E_\gamma} \right)^4 \text{GeV}^{-1} \text{s}^{-1}, \quad \text{for } E_\gamma \geq Q \quad (40)$$

where $Q \simeq 4 \times 10^4 (\tau/1 \text{ s})^{-1/3} \text{ GeV}$ is the energy of the peak quark flux averaged over the last τ seconds of the PBH's evaporation lifetime [4]. The Linton et al. parameterization was derived by performing the convolution of

Equation 26 with an approximation to the quark emission rate which replaces the energy dependence of Figure 7 with a delta function at Q . Equation 39 is reasonably accurate for low energies but, for $E_\gamma > 0.1Q$, differences of up to 30% appear. More seriously, at $E_\gamma = Q$, the functional form of Equation 39 drops to zero, which is not the actual behavior. Equation 40 matches the photon emission rate reasonably to within 20% for $Q \leq E_\gamma < 2Q$ but strongly overestimates the exponential fall off in the emission rate at the highest energies.

2.6. The Time-Integrated Photon Spectrum

In Section 3 we consider strategies for direct PBH burst searches at VHE gamma-ray observatories. One strategy is to utilize the photon time-integrated energy spectrum, i.e., the instantaneous photon emission rate integrated over a time interval from an initial remaining evaporation lifetime $t = \tau$ to the completion of evaporation at $t = 0$, as a function of energy,

$$\left[\frac{dN_\gamma}{dE_\gamma} \right]_\tau = \int_0^\tau \frac{d^2 N_\gamma}{dE_\gamma dt} dt. \quad (41)$$

Figure 11 shows the photon time-integrated energy spectra for $\tau = 0.01, 0.1, 1.0, 10.0,$ and 100.0 s using our parameterizations of Section 2.5. In Figure 11, it can be seen that $[dN_\gamma/dE_\gamma]_\tau$ obeys different power laws above and below a transition energy $E_{\text{tr}}(\tau)$ which is of order $kT_{BH}(\tau)$: for $E_\gamma < E_{\text{tr}}$, $[dN_\gamma/dE_\gamma]_\tau \propto E_\gamma^{-1.5}$ and for $E_\gamma > E_{\text{tr}}$, $[dN_\gamma/dE_\gamma]_\tau \propto E_\gamma^{-3.0}$.

To understand the origin of these slopes, we first change the variable of the integration in Equation 41 from t to $x(t) = E/kT_{BH}(t)$ where $kT_{BH}(t) = E_0(\tau_0/t)^{1/3}$ is given by Equation 22 with $E_0 = 7800$ GeV and $\tau_0 = 1$ s. Thus $dt = 3\tau_0(E_0/E)^3 x^2 dx$ and

$$\left[\frac{dN_\gamma}{dE} \right]_\tau = 3\tau_0 \left(\frac{E_0}{E} \right)^3 \int_0^{x(\tau)} \psi_\gamma(x'_\pi) x'^2 dx' \quad (42)$$

for a directly Hawking-radiated species. The integral in Equation 41 is dominated at high E_γ by the directly Hawking-radiated photons and so Equation 42 implies $[dN_\gamma/dE_\gamma]_\tau \sim E_\gamma^{-3}$ for high E_γ ; this result reflects the fact that approximately $\tau \propto T_{BH}^{-3}$. The integral in Equation 41 is dominated below $E_\gamma \sim kT_{BH}$ by the fragmentation function which must be convolved with Equation 42 and gives $[dN_\gamma/dE_\gamma]_\tau \sim E_\gamma^{-3/2}$ for $E_\gamma \lesssim kT_{BH}$; this result reflects the fact that the fragmentation function Equation 30 behaves as $z_\gamma^{-3/2}$ for $z_\gamma \rightarrow 0$.

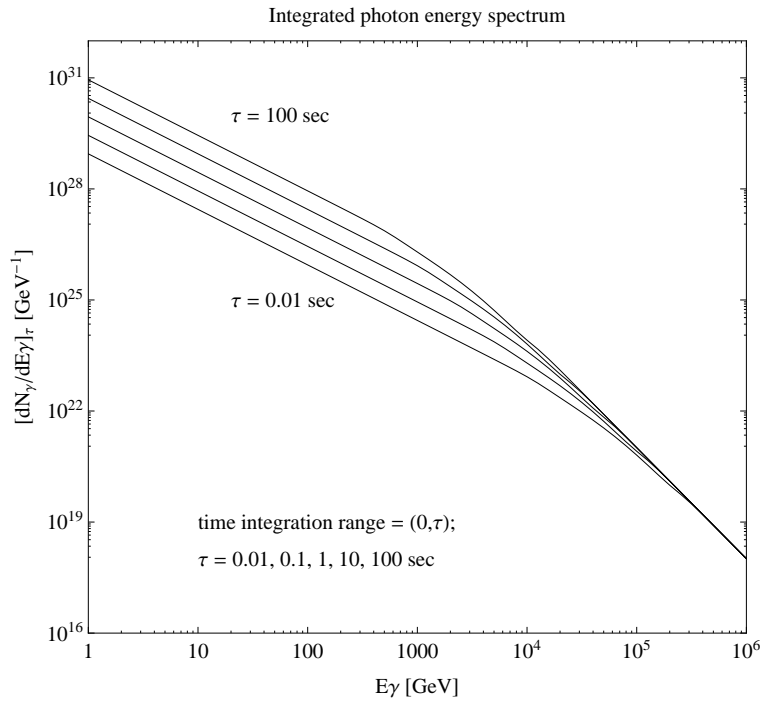


Figure 11: The photon spectrum, integrated over the final evaporation lifetime interval $\tau = 100, 10, 1, 0.1$ and 0.01 s.

A parameterization for the time-integrated photon spectrum, derived by fitting the HERWIG-based Monte Carlo simulations of the photon flux from $1 \text{ GeV} \leq T_{\text{BH}} \leq 100 \text{ GeV}$ black holes of reference [14], was published by Bugaev et al. [34; 35],

$$\frac{dN_\gamma}{dE_\gamma} \approx 9 \times 10^{35} \begin{cases} \left(\frac{1 \text{ GeV}}{T_\tau}\right)^{3/2} \left(\frac{1 \text{ GeV}}{E_\gamma}\right)^{3/2} & \text{GeV}^{-1} \text{ for } E_\gamma < kT_\tau \\ \left(\frac{1 \text{ GeV}}{E_\gamma}\right)^3 & \text{GeV}^{-1} \text{ for } E_\gamma \geq kT_\tau \end{cases} \quad (43)$$

for $E_\gamma \gtrsim 1 \text{ GeV}$. Here T_τ is the temperature of the black hole at the beginning of the final burst time interval, i.e., $T_\tau = T_{\text{BH}}(\tau)$ as given by Equation 22. This approximation agrees well with our calculations of the time-integrated spectrum based on the pion fragmentation model, Equation 25, and shown in Figure 11. Either could be used as input for comparing the experimental sensitivities of different VHE gamma-ray observatories to a time-integrated PBH signal.

2.7. PBH Burst Light Curve

We now consider the time dependence of the BH burst, i.e., the final ‘‘chirp’’. In Section 3 we explore whether knowledge of the time dependence can be used to enhance statistical significance in a PBH search.

To find the time evolution of the BH burst, we integrate the differential emission rate $d^2N_\gamma/(dE_\gamma dt)$ over photon energy E_γ while retaining the time dependence. Hence the burst emission time profile (at the source) is

$$\left[\frac{dN_\gamma}{dt}\right]_{\text{Emission}} = \int_{E_{\text{min}}}^{E_{\text{max}}} \frac{d^2N_\gamma}{dE_\gamma dt} dE_\gamma. \quad (44)$$

In general E_{min} and E_{max} are set by the energy range of the detector. Figure 12 shows the BH burst emission time profile in the energy range $50 \text{ GeV} \leq E_\gamma \leq 100 \text{ TeV}$.

It is interesting to relate the photon time profile to the total luminosity function of the BH. By basic thermodynamics, the luminosity $dE/dt \propto T_{\text{BH}}^4 4\pi R^2$ per emitted mode. For a Schwarzschild black hole, the radius $R \propto M_{\text{BH}}$ and $T_{\text{BH}} \propto 1/M_{\text{BH}}$, and so $dE/dt \propto T_{\text{BH}}^2$ for the directly Hawking-radiated particles. Because the average energy of the directly Hawking-radiated particles is $\bar{E} \propto T_{\text{BH}}$, we expect for the directly Hawking-radiated particles that $dN/dt \sim \bar{E}^{-1} dE/dt \propto T_{\text{BH}}$. To estimate the τ dependence of dN_γ/dt , we note that the photon emission spectrum is dominated by the

fragmentation component. The fragmentation function Equation 25 implies a multiplicity (number of final states per initial particle) proportional to $T_{BH}^{1/2}$. Convolving the multiplicity dependence with the dN/dt dependence per Hawking-radiated state leads to $dN_\gamma/dt \propto T_{BH}^{3/2} \propto \tau^{-1/2}$, in agreement with the power law of approximately -0.5 found in Figure 12. We also note that, because energy is conserved in the fragmentation and hadronization process, the total BH luminosity summed over all final state species is approximately $dE/dt \propto \tau^{-2/3}$.

The dependence of the BH burst emission time profile on the energy range (E_{\min}, E_{\max}) is also relevant. Figure 13 shows dN_γ/dt calculated using several (E_{\min}, E_{\max}) energy bands between 0.1 GeV and 1000 TeV. We see that the low energy bands between 0.1 GeV and 10 TeV have similar emission profiles. However, above energies of ~ 10 TeV the burst emission time profile is energy-dependent and has an inflection region occurring ~ 1 s to 0.1 s before the end of the BH evaporation lifetime. This energy dependence can be seen in the bottom panel of Figure 13, where we have plotted several energy bands above 10 TeV. The energy dependence of the burst emission time profile can be understood by referring to Equations 32 and 36 and Figure 10. At low energies (below the inflection region), the photons generated by the Hawking-radiated quarks and gluons dominate the flux; at high energies (above the inflection point), the directly Hawking-radiated photons dominate the flux. In the inflection region, the two components are comparable.

Figures 12 and 13 display the emission time profiles, i.e., the source emission rate as a function of remaining time. Let us now consider the detection time profile, i.e., the *light curve* of the PBH burst for a specific VHE gamma-ray observatory. The detection time profile can be calculated from

$$\left[\frac{dN_\gamma}{dt} \right]_{\text{Detection}} = \frac{1}{4\pi r^2} \int_{E_{\min}}^{E_{\max}} A(E_\gamma) \frac{d^2 N_\gamma}{dE_\gamma dt} dE_\gamma \quad (45)$$

where $A(E_\gamma)$ is the effective area of the detector, as a function of photon energy E , and r is the distance from the PBH to the detector.

In this paper, we will use the HAWC observatory [13] as a representative VHE gamma-ray observatory to investigate the PBH observational signatures. Figure 14 shows the detection time profile for a PBH burst at a distance $r = 0.015$ parsecs, in the HAWC energy range (50 GeV — 100 TeV) and for the HAWC effective area published in reference [36]. If the actual local PBH density is equal to the present limit on the local PBH density

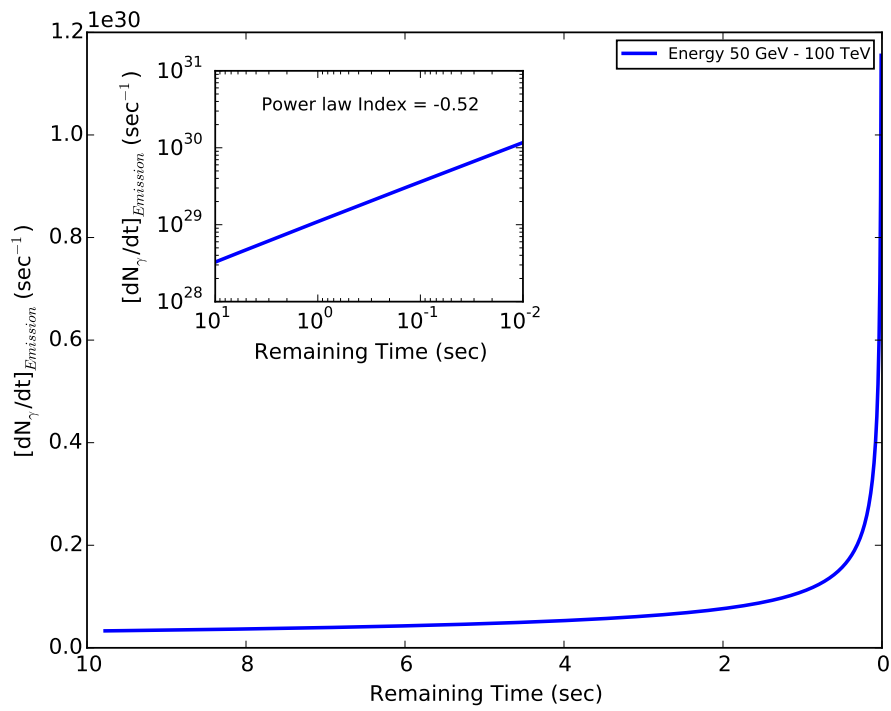


Figure 12: The BH burst emission time profile, the emission rate integrated over energy, for the energy range 50 GeV – 100 TeV. As discussed in the text, this shape is well described by a power law with a index of ~ -0.5 .

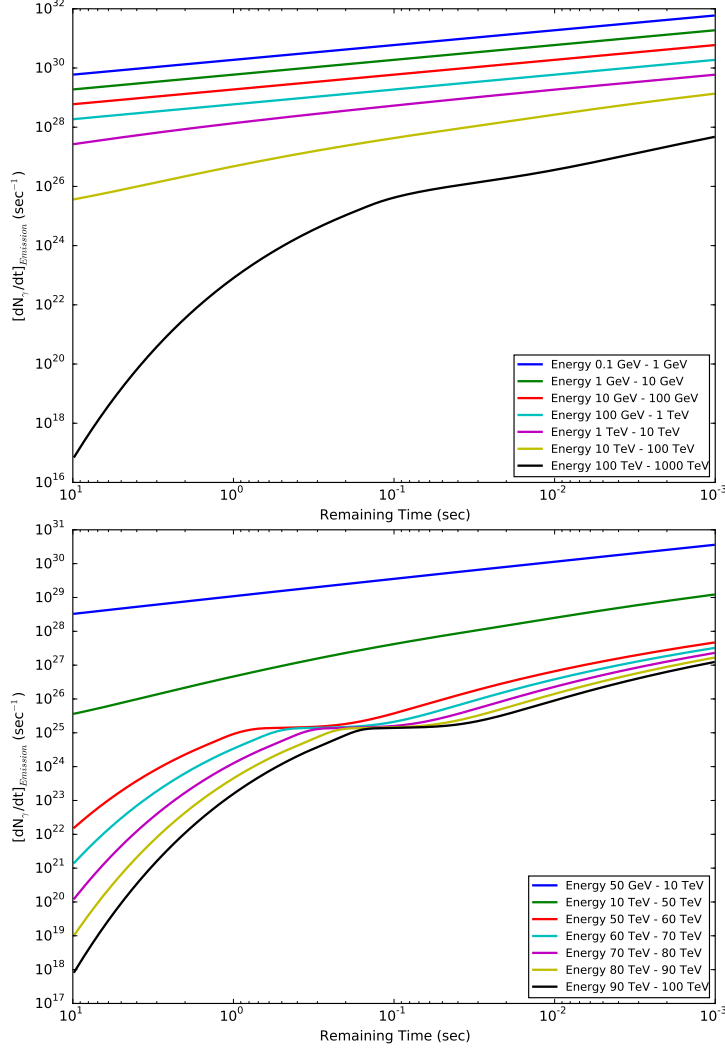


Figure 13: Top panel shows the BH burst source emission time profile, the emission rate integrated over energy, for various integrated energy ranges. Here the shape of the emission time profile is the same for energy bands less than ~ 10 TeV but is starting to become energy-dependent above ~ 10 TeV. Bottom panel shows the BH burst source emission time profile for a number of energy bands above 10 TeV. Here the energy dependence of the burst profile for higher energy bands can be clearly seen with a inflection region around $\tau \sim 0.1$ s.

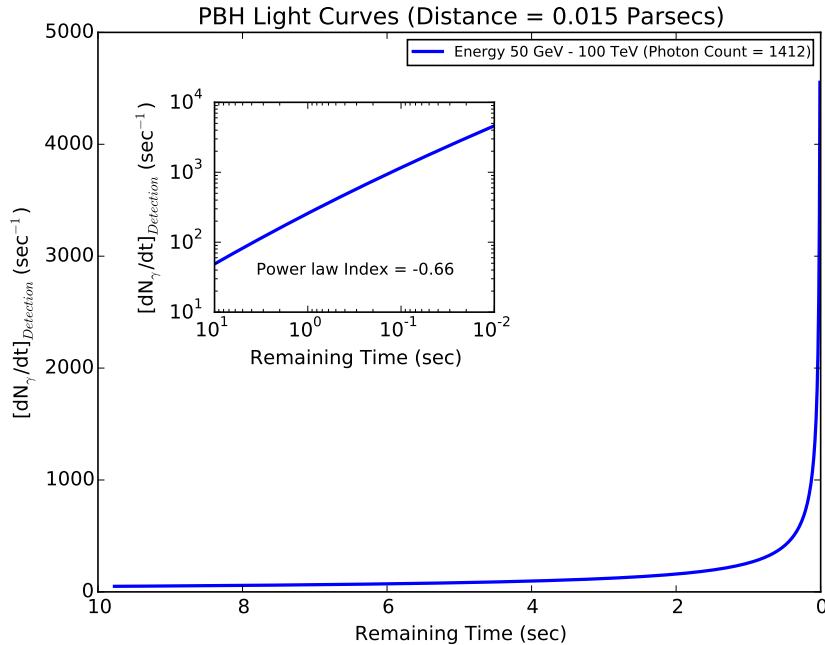


Figure 14: Simulated PBH burst light curve observed by HAWC (at a distance of 0.015 parsecs) obtained by convolving with the HAWC effective area published in Ref [36]. This shape is well described by a power law with a index of ~ -0.7 .

(shown in Figure 20), HAWC might expect to have a 30% chance of observing such a burst (at 0.015 pc or closer) within its instantaneous field of view during 5 years of data taking.

An interesting feature of the BH signal is that the detection time profile (Figure 14) rises more rapidly than the source emission time profile (Figure 12) as the remaining evaporation lifetime $\tau \rightarrow 0$. This occurs because the effective area $A(E_\gamma)$ is largest at high photon energies, $E_\gamma > 10$ TeV, where both direct and fragmentation photon components are important but have different energy dependencies.

The HAWC detection time profiles for various photon energy ranges, analogous to the burst emission time profiles shown in the bottom panel of Figure 13, are displayed in Figure 15.

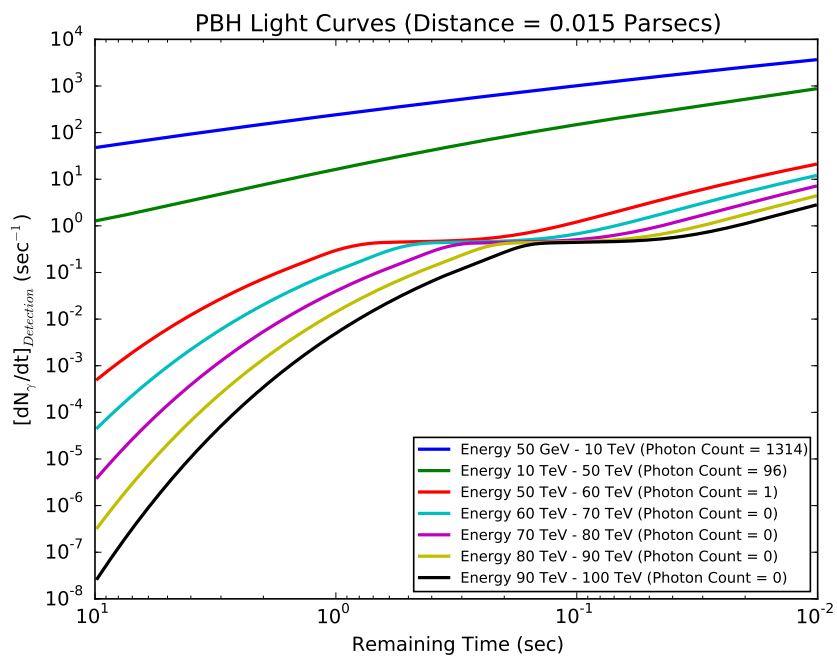


Figure 15: Simulated detection time profiles of a PBH burst at a distance of 0.015 parsecs observed by HAWC in multiple energy bands. Photon numbers detected in each energy band are shown in the legends.

3. PBH Burst Search and Upper Limits

3.1. PBH Burst Simple Search

The most straightforward way to search for a PBH burst (or any burst) is to define search windows for the data both in time and space (i.e., angular position on the sky) and then to inspect the search windows for excess over the expected background. The manner in which the search intervals are defined, and the threshold level set, varies with different searches. For a given detector, this Simple Search method can be divided into two categories: a blind untriggered search and an externally triggered search. In the blind search, the location and time of the burst is not *a priori* known, and hence all spatial and temporal windows need to be inspected for an excess over the background. This may incur a large number of trials and correcting for them may reduce the sensitivity of the search. An externally triggered search, on the other hand, will look at a certain sky position and time for a burst once the burst has been detected in another detector. Depending on how accurately the location of the externally triggered burst is known, a triggered search can incur typically one or a few trials, significantly less than the blind search.

For both categories of Simple Search, we need to estimate the minimum number of expected signal counts, μ_o , required for a statistically significant burst detection to be probable. The value μ_o may depend on the duration of the search window and its location in the detector's field. In order to calculate μ_o , fluctuations in the background and fluctuations in the signal need to be considered. Let n be the number of counts which has a probability of being due to random fluctuation of the background of less than $p_0 \sim 2.87 \times 10^{-7}$ (corresponding to 5σ), after correcting for N_t trials. If the detector counts follow a Poisson distribution and B is the mean number of background counts expected over the search window Δt , then n is found from

$$p_c = p_o/N_t = P(\geq n|B). \quad (46)$$

Here p_c is the required p-value after correction for N_t trials. The notation $P(\geq n|B)$ represents the Poisson probability of getting n or more counts when the Poisson mean is B . To estimate μ_o , we also need to consider the fact that the signal will fluctuate around some mean to produce n counts including background in the detector. Thus, we need to find the mean value of the signal that together with the background will give us the desired n counts in the detector $X\%$ of the time. The signal mean is then our μ_o value.

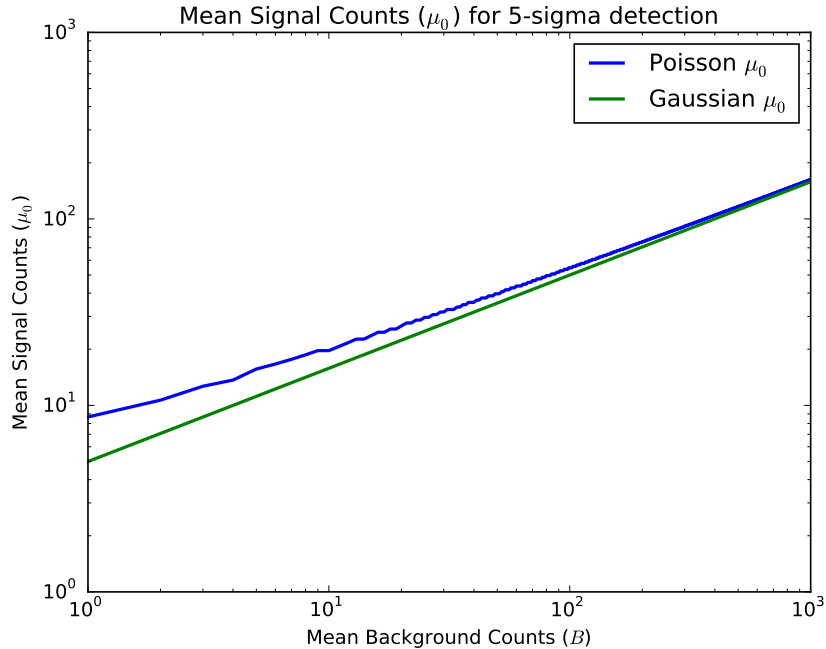


Figure 16: Number of signal counts needed (μ_\circ) for a 5σ detection 50% of the time for a single trial as a function of the background counts (upper blue line). The μ_\circ values in the case of a Gaussian distribution is also shown (lower green line).

In typical searches, $X\%$ is taken to be 50%; that is, μ_\circ is defined as the signal strength needed to give a 5σ detection 50% of the time. Hence, for a Simple Search, we can estimate μ_\circ from the equation

$$P(\geq n|(B + \mu_\circ)) = 0.5. \quad (47)$$

Note that with these definitions, $\mu_\circ \approx n - B$ is a reasonable approximation. Figure 16 shows the mean signal counts, μ_\circ , for a 5σ detection 50% of the time for a single trial as a function of background counts, based on this PBH Simple Search method. The μ_\circ values that we would get for a Gaussian distribution are also shown.

3.2. Binned Maximum Likelihood (ML) Search

The Simple Search methods of Section 3.1 use all photons detected in the search window irrespective their energy or time profile. Thus, the Sim-

ple Search method does not make use of the time profile (the light curve dN_γ/dt) or the energy profile (dN_γ/dE) of the PBH burst which we derived in Section 2. Does utilizing the time profile of the final seconds of the burst, which we calculated in Section 2.7, improve search sensitivity? To address this question, we investigate the binned Maximum Likelihood search method using a simple Monte Carlo simulation.⁸

Consider a search window of duration Δt . Each search window has an expected background mean (B), and possibly signal mean (S). The background counts are expected to be distributed over Δt with uniform probability while the PBH signal counts are expected to be distributed according to Figure 14. In a binned Maximum Likelihood search we take advantage of the PBH burst time profile by dividing each search window into k bins of time. If there is a PBH burst in a given window then we expect the signal to be distributed in these k bins according to Figure 14. For the purposes of comparison with the Simple Search, we will imagine that in both the Simple Search and the ML search the search window Δt ends at the expiration of the PBH burst, giving each search the best possible alignment of the search window. Thus, for a given search window, we can write the log of the likelihood ratio of the signal-plus-background hypothesis to the background-only hypothesis as

$$\lambda = \sum_i^k \ln \frac{P(c_i | (s_i + b_i))}{P(c_i | b_i)} \quad (48)$$

where c_i is the observed number of counts in each bin, s_i and b_i are the expected (mean) number of signal and background counts respectively in each bin ($S = \sum_i^k s_i$ and $B = \sum_i^k b_i$), and $P(c|q)$ is the Poisson probability of obtaining c counts when q counts are expected.

Proceeding further, we have

$$\lambda = \sum_i^k \left(\ln \frac{(s_i + b_i)^{c_i} e^{-(s_i + b_i)}}{c_i!} - \ln \frac{b_i^{c_i} e^{-b_i}}{c_i!} \right)$$

⁸We also note that the energy profile of the burst may improve the search sensitivity. For example, the background of the detector may vary with the energy, and the detector may be more sensitive in certain energy ranges. However, we defer investigation of energy profile considerations to a separate paper.

which simplifies to

$$\lambda = \sum_i^k c_i \ln \left(\frac{s_i + b_i}{b_i} \right) - \sum_i^k s_i = \sum_i^k c_i \ln \left(1 + \frac{s_i}{b_i} \right) - S. \quad (49)$$

If a non-zero signal occurs in a search window, then we estimate its strength as \hat{S} , the value of S which maximizes λ , as shown in the top panel of Figure 17. (In Figure 17, λ as a function of the expected signal S is shown for a single simulated randomized search window with $\hat{S} = 25$.) The value of λ associated with \hat{S} is denoted by $\hat{\lambda}$. The maximum signal location can be found by partially differentiating the log likelihood function Equation 49 with respect to S ,

$$\frac{\partial \lambda}{\partial S} = \sum_i^k \left(\frac{c_i}{s_i + b_i} \right) \frac{\partial s_i}{\partial S} - 1 \quad (50)$$

Setting $s_i = S f_i$ where f_i is the normalized binning of the PBH light curve shown in Figure 14, we find

$$\frac{\partial \lambda}{\partial S} = \sum_i^k \left(\frac{c_i f_i}{S f_i + b_i} \right) - 1 \equiv Q(S) - 1. \quad (51)$$

For λ to be a maximum at $S = \hat{S}$, we require $\partial \lambda / \partial S = 0$ at $S = \hat{S}$ and so

$$Q(\hat{S}) = \sum_i^k \left(\frac{c_i f_i}{\hat{S} f_i + b_i} \right) = 1. \quad (52)$$

Because Equation 52 is not analytically solvable, we numerically evaluate $Q(S)$ and $Q(\hat{S})$, as shown in the bottom panel of Figure 17. Because $Q(S)$ is monotonically decreasing, we employed an efficient binary search algorithm to find \hat{S} .

In order to find μ_0 , the mean number of expected signal counts necessary for a probable statistically significant detection for the binned Maximum Likelihood search method, we need two levels of simulation. First, we perform a background-only simulation to obtain the distribution of λ for background only, and determine λ_0 , the value corresponding to p_c , the p-value for 5σ significance, as for the Simple Search. We then perform a second set of simulations, varying the expected signal mean until the ML search finds

$\hat{\lambda} > \lambda_0$ half the time, i.e., with probability 0.5. For the background-only simulation, $\hat{\lambda}$ is used as a test statistic instead of the signal strength \hat{S} because, although there is a correlation between $\hat{\lambda}$ and \hat{S} , the log likelihood ratio $\hat{\lambda}$ more explicitly answers the question, “is this search more signal-like than background-only-like”.

For our ML search, we chose k time bins of equal duration. In the background-only simulation, we generate events in each bin using $c_i \sim Pois(k^{-1}B)$, where k is the number of bins, B is the expected background mean, and the notation $c_i \sim Pois(\beta)$ indicates c_i is a random number generated from a Poisson distribution with mean β . For each such simulated search we find and record $\hat{\lambda}$. The procedure is repeated a large number of times to find the value λ_0 which has a p-value corresponding to 5σ Gaussian significance. This defines our criterion for a detection.

For the signal-plus-background simulation, we run simulations with signal mean S and vary S until the search finds $\hat{\lambda} > \lambda_0$ 50% of the time. For the signal-plus-background simulation, the number of events in each bin is generated according to

$$c_i^{sim} \sim Pois(Sf_i + \frac{B}{k}) \quad (53)$$

The simulation process is illustrated in Figure 18. A good starting estimate for S is the value corresponding (on average) to λ_0 , which itself can be estimated by recording the \hat{S} values during the background-only simulation.

The results of the Maximum Likelihood simulation compared with the PBH burst Simple Search are shown in Figure 19. For a value of B corresponding roughly to the conditions of the HAWC 10 second expected limit in reference [13], the ML search method would produce an upper limit approximately a factor of 1.3 better than the Simple Search, using the detector-related methods which we describe below in section 3.3 [13].

We have also investigated an unbinned Maximum Likelihood search using the complete unbinned time profile (“chirp”) of the PBH signal. The unbinned search, however, results in little gain compared to a $k = 10$ bin search under the conditions of the present study, namely moderate background events (less than 50) in the search window, and the simplifying assumption that we externally know the burst time. Further studies are under way and will be reported in a separate paper.

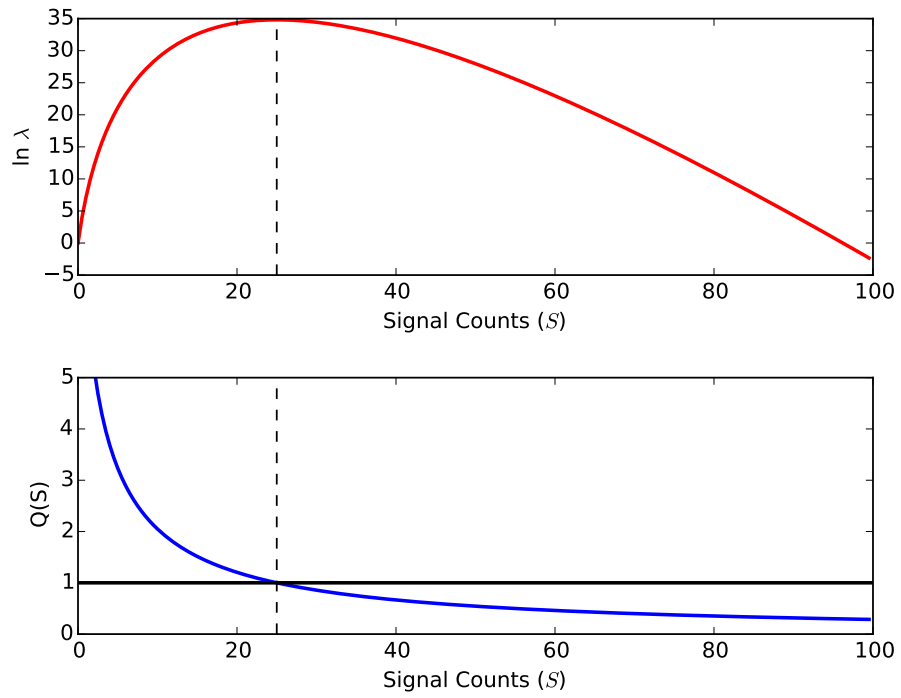


Figure 17: Log likelihood ratio (upper panel) and $Q(S)$ (lower panel) as a function of S for a simulated ML search bin with $\hat{S} = 25$. The log likelihood ratio is a maximum, i.e., $S = \hat{S}$, where the function $Q(S) = 1$.

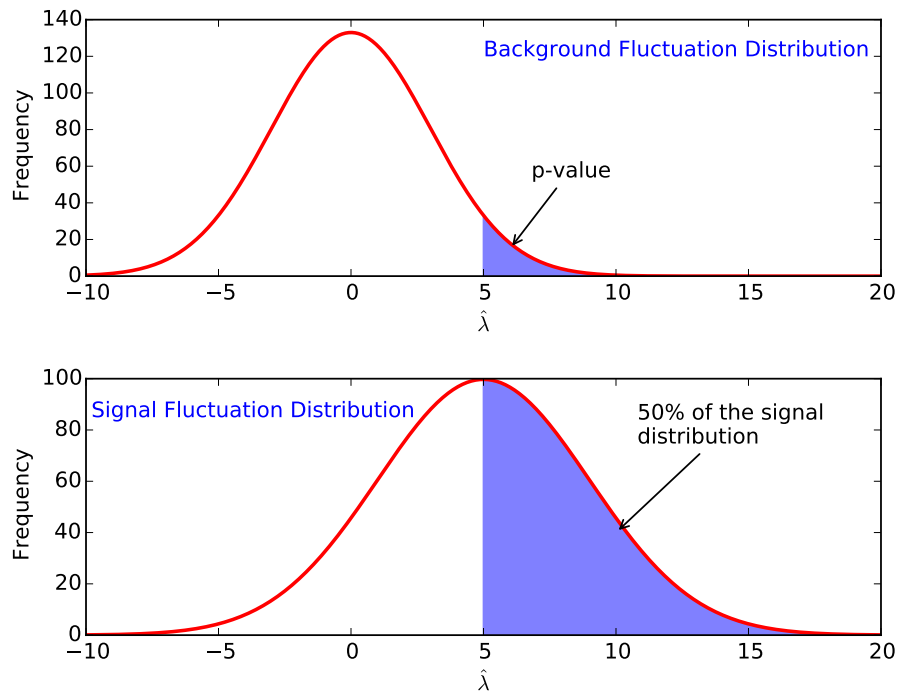


Figure 18: The number of mean signal counts (μ_0) needed for a 5σ detection 50% of the time is found by first simulating many background-only searches. From the resulting distribution of the maximum log likelihood $\hat{\lambda}$ values (upper panel), we find the value required ($\lambda_0 = 5$ in this case) for the desired p-value. We then simulate many searches containing both signal and background events. In the bottom panel we show the distribution of the test statistic $\hat{\lambda}$ for the case employing an average of μ_0 signal events per search; in this case the searches produce $\hat{\lambda} > \lambda_0 = 5$ with a probability of 50%. A smaller value of the expected signal would give a smaller fraction of searches passing the $\hat{\lambda} > \lambda_0$ criterion.

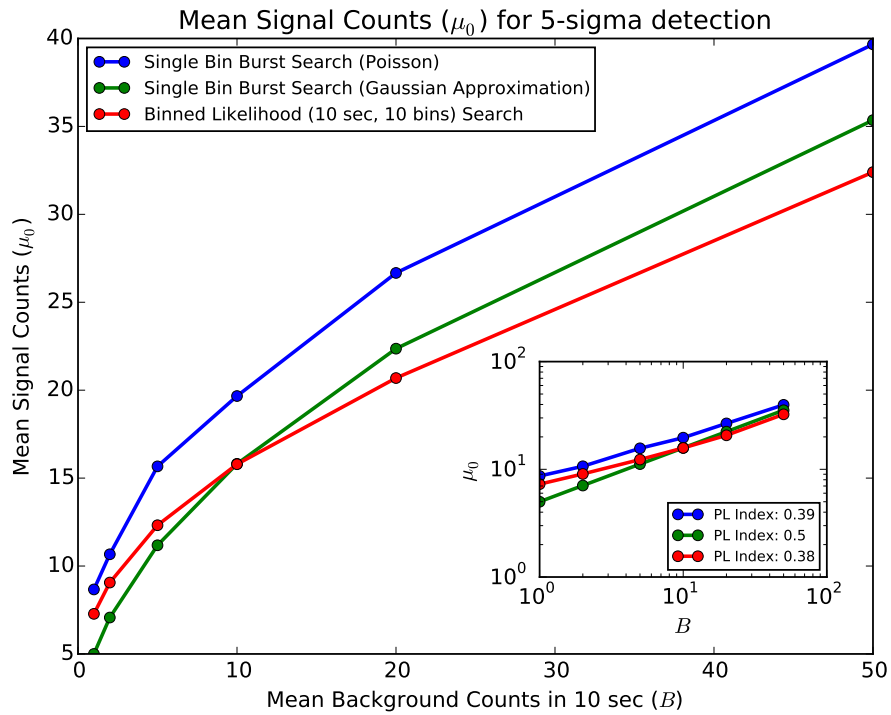


Figure 19: Comparison of the two PBH burst search methods investigated in this paper: the Simple Search method and the binned Maximum Likelihood method. The legend denotes the curves at large B in top to bottom order (blue, red, green). The insert shows that the power law (PL) index of the dependence of μ_0 on B . Both search methods have similar power law dependencies.

3.3. PBH Upper Limit Estimation

In the case of a null detection (i.e., if no PBH bursts are observed), we can derive an upper limit on the local PBH burst rate density, i.e., the number of PBH bursts per unit volume per unit time in the local solar neighborhood. To calculate the upper limit, the PBH detectable volume for a given detector is needed. The expected number of photons received by a detector at or near Earth from a PBH burst during the last τ seconds of its evaporation lifetime at a non-cosmological distance r and at detector angle θ is

$$\mu(r, \theta, \tau) = \frac{(1-h)}{4\pi r^2} \int_{E_1}^{E_2} \frac{dN_\gamma(\tau)}{dE_\gamma} A(E_\gamma, \theta) dE_\gamma. \quad (54)$$

In this expression, $dN_\gamma(\tau)/dE_\gamma$ is the PBH photon emission energy spectrum integrated from a remaining burst lifetime $\tau' = \tau$ to $\tau' = 0$. We implicitly assume that the search window Δt has been chosen to end at or near $\tau' = 0$. The function $dN_\gamma(\tau)/dE_\gamma$ can be approximated using Equation 43. The energies E_1 and E_2 are the lower and upper bounds, respectively, of the energy range of the detector, h is the dead time fraction of the detector, and $A(E_\gamma, \theta)$ is the effective area of the detector as a function of E_γ and θ . The detector angle θ can be the zenith angle for ground-based detectors or the bore sight angle for space-based detectors. The function $A(E_\gamma, \theta)$ is typically obtained from a simulation of the detector.

In Sections 3.1 and 3.2, we estimated the minimum number of expected signal counts needed for a detection, μ_0 . By setting μ_0 equal to $\mu(r, \theta, \tau)$, the expected number of counts from a PBH burst at a distance r from Earth, we can solve Equation 54 to find the maximum distance from which a given detector can detect a PBH burst,

$$r_{\max}(\theta, \tau) = \sqrt{\frac{(1-f)}{4\pi\mu_0} \int_{E_1}^{E_2} \frac{dN(\tau)}{dE_\gamma} A(E_\gamma, \theta) dE_\gamma}. \quad (55)$$

The total PBH detectable volume of the detector is then

$$V(\tau) = \sum_{\theta} V(\theta, \tau) = \frac{4}{3}\pi \sum_{\theta} r_{\max}^3(\theta, \tau) \frac{\text{FOV}_{\text{eff}}(\theta)}{4\pi}, \quad (56)$$

where $\text{FOV}_{\text{eff}}(\theta)$ is the effective field-of-view associated with the detector angle θ and the summation is over the bands of θ of the detector [13].

If PBHs are uniformly distributed in the solar neighborhood and, at the $Y\%$ confidence level, zero PBH bursts are observed, then the $Y\%$ confidence level upper limit (UL_Y) on the rate density of PBH bursts can be estimated as

$$UL_Y = \frac{m}{V\Pi}. \quad (57)$$

Here V is the effective PBH detectable volume, Π is the total search duration (typically in years) and m is the upper limit on the expected number of PBH events given that at the $Y\%$ confidence level zero bursts are observed. Note that for Poisson fluctuations, $P_{\text{Poisson}}(0|m) = m^0 e^{-m}/0! = 1 - Y$ implies that $m = \ln(1/(1 - Y))$. For $Y = 99\%$, $m = \ln 100 \approx 4.6$ and hence the upper limit on the PBH burst rate density in the case of null detection will be

$$UL_{99} = \frac{4.6}{V\Pi}. \quad (58)$$

Figure 20 shows published PBH burst rate density 99% CL upper limits and sensitivities for various experiments. The PBH rate density limits calculated for Milagro and projected for HAWC are strictest around search window durations of 1 second and 10 second respectively. These optimum burst search intervals reflect the characteristics of the observatory and dependence of the background.

Let us understand the general features of Figure 20, which shows limits as a function of search window, Δt . From Equations 55–58, we can see that UL , the upper limit on the local PBH rate density, scales as

$$UL \sim (\mu_0(\Delta t)/N_\gamma(\tau))^{3/2} \quad (59)$$

where μ_0 is the sensitivity for a given search window Δt , and $N_\gamma(\tau)$ is the number of observable photons produced by the source over its remaining burst lifetime τ . Better sensitivity corresponds to smaller μ_0 , the number of signal photons required for detection of a signal, and a stricter PBH limit. For a source at a given distance (e.g., the one at the outer edge of the volume considered), $N_\gamma(\tau)$ decreases when the search window is shorter, and produces a weaker PBH limit. Shorter search windows incur less background events but also see fewer source photons. In this case, μ_0 is dominated by statistical fluctuations, in particular those associated with the detector background rate, i.e., from Figure 19 $\mu_0 \propto B^{0.38} \propto (\Delta t)^{0.38}$; and $N_\gamma(\tau)$ is determined by the integral of the PBH time profile, slightly modified by the energy-dependent effective area of the detector, i.e., from 14 $N_\gamma(\tau) \propto$

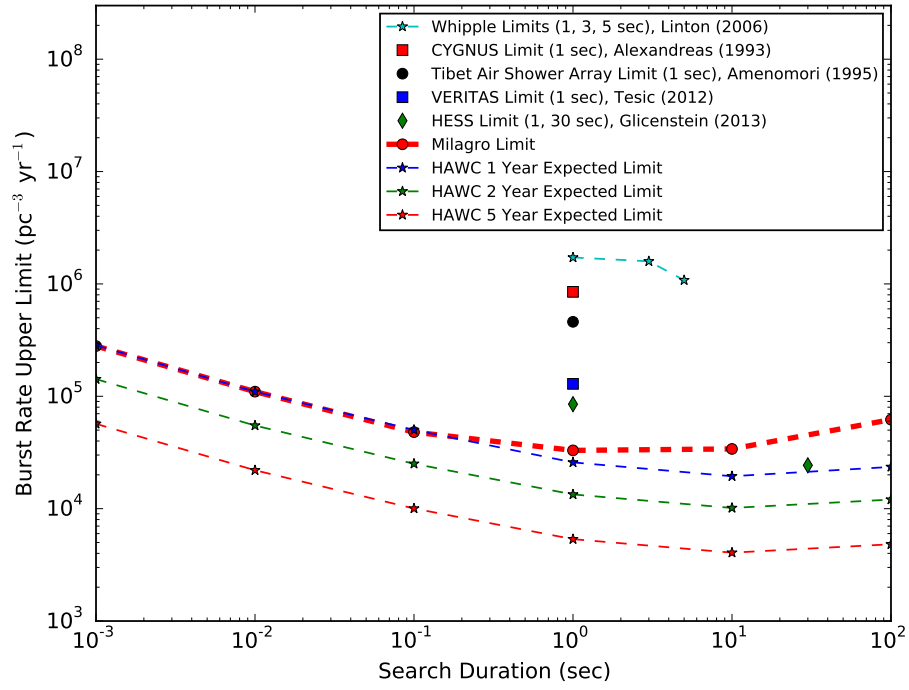


Figure 20: Published PBH Burst Rate Density 99% CL Upper Limits and sensitivities for various experiments [13; 7; 8; 9; 10; 11; 12].

$\int_0^\tau t^{-0.66} \propto (\Delta t)^{0.34}$. These dependencies of μ_0 and $N_\gamma(\tau)$ are both power laws and, despite their very different physical origins, nearly cancel. Secondary effects such as the larger number of trials incurred for shorter search windows ($N_t \propto 1/\Delta t$), and the ability to optimize background rates for larger Δt (for which the detection efficiency is higher) give the Δt -dependence seen in Figure 20.

Thus, in summary, the shape of the PBH limit curves will be similar but will need to be evaluated for each gamma-ray detector. The improvements suggested in this paper, of including the energy and time dependence of the PBH signal, will typically decrease the required μ_0 . We anticipate that the PBH burst rate density limit may particularly improve at longer search windows Δt as a result.

4. Differentiating the PBH Burst from Other GRBs

Another important question regarding PBH burst detection is how to differentiate a PBH burst from commonly detected GRBs of known cosmological origin. In particular, some short GRBs of duration less than 2 seconds have light curves which are very similar to the BH burst emission time profile shown in Figure 12.

Multi-wavelength observations are very important in differentiating PBH bursts from other known GRB source types. Almost all GRBs have low-energy or VHE afterglows of recognizable shape following the main gamma-ray burst. In the case of a PBH burst, no afterglow is expected once the BH gamma-ray burst has expired, with the possible exception of an afterglow generated if the PBH is embedded in a sufficiently dense ambient plasma or magnetic field [3]. The prompt burst time profile in various energy bands may also be used to distinguish a PBH origin. The light curve from a BH burst occurring in free space is not expected to exhibit multi-peak structure at detector energies: for an isolated PBH a single short peak as shown in Figure 12 is expected. Moreover, the extension of cosmological GRB spectra into TeV energies is uncertain because of the attenuation of gamma-rays from distant GRBs by pair-production off the intergalactic medium (IGM) and the possibility of a cutoff in the GRB source spectrum [37; 38]. In contrast, local PBH bursts have a spectrum which extends well above 1 TeV during the latter parts of the BH burst (for intervals as long as 100 s). The predicted BH burst emission time profile has a relatively hard power law index of ~ -0.5 which is significantly harder than most known gamma-ray

sources at high energy. Current instruments are sensitive to local PBH bursts (< 1 parsec) [13], where the ISM is not expected to significantly attenuate TeV photons. Thus, detection in TeV observatories, together with the other characteristics expected for a BH burst, will lead to a potentially unique identification of the PBH signal.

In addition, GRBs due to PBH bursts are not expected to be accompanied by gravitational wave radiation. GRBs from other sources may be accompanied by gravitational waves (GW) and for short GRBs, a GW signature would confirm a compact star merger origin (which is the leading model for short GRBs). Moreover, we expect the emission of a neutrino burst and cosmic-ray (e^\pm , p , \bar{p} and possibly n) burst of similar time profiles to accompany the gamma-ray radiation in the event of a BH burst. These neutrino and cosmic-ray bursts should be emitted simultaneously by the BH with the gamma-ray burst. Thus far the reason that we have not detected neutrinos from standard GRBs may be due to their great distances. However, any PBH burst candidate that we detect with the current instruments should be very local, and so UHE neutrino and/or cosmic-ray telescopes may possibly detect the accompanying neutrino or cosmic-ray bursts from the PBH [39; 15]. Table 1 summarizes the observational differences between standard cosmological GRBs and PBH bursts.

Gamma-ray Bursts (GRB)	PBH Bursts
Detected at cosmological distances	Unlikely to be detected outside our Galaxy
Time duration can range from fraction of second to few hours	Time duration is most likely less than few seconds
May have multi-peak time profiles	Single-peak time profile
Typically a single peak shows Fast Rise Exponential Decay (FRED) time profile	Power-law Rise Fast Fall (PRFF) time profile expected
X-ray, optical, radio afterglows are expected	No multi-wavelength afterglow is expected
Most GRBs show hard-to-soft evolution	Soft-to-hard evolution is expected from PBH bursts
Cosmic-rays are not expected to arrive from GRBs	Cosmic-ray bursts are expected from nearby PBH bursts
Gravitational wave signal is expected	No gravitational wave signal is expected
Neutrino burst may be seen	Simultaneous neutrino burst may be seen from nearby PBH
TeV radiation may be cut off either at the source or by the intergalactic medium	TeV signal is expected during the last seconds of the burst

Table 1: A summary of potential observational differences between standard cosmological GRBs and PBH bursts

5. Discussion

This paper assumes the Standard Evaporation Model (SEM) of black hole radiation based on the Standard Model of high-energy physics and the Hawking radiation of fundamental particle species, such as quarks and gluons, as initially asymptotically free particles. In particular, our analysis of search methods in Section 3 is based on the SEM. If a direct PBH burst search is unsuccessful, the null result will set an upper limit on the local density of such PBH burst events. Any derived limit will also depend on the validity of the SEM. Alternative emission theories make different predictions for the PBH photon emission rate and/or spectrum. Here we discuss some issues arising from our SEM-based analysis.

5.1. The Pion Fragmentation Function for Quarks and Gluons

In this paper, we assumed that all Hawking-radiated quarks and gluons fragment and hadronize into pions, according to the fragmentation function in Equation 25. Is the pion fragmentation function employed in Section 2 a realistic approximation?

Fragmentation functions have been extracted from accelerator data, e.g. from electron-positron collider experiments. The heuristic model in Equation 25 agrees qualitatively with the empirical fragmentation functions [28], although the quantitative accuracy is limited. Two aspects of the fragmentation process are absent from the heuristic model. Firstly, the assumption that all flavors of quarks eventually fragment equally and completely into pions is not strictly true. The fragmentation steps will also produce other mesons and baryons. In addition, heavy particles such as the top quark, W^\pm , Z^0 and H initially decay into lighter quarks rather than directly undergoing hadronic fragmentation into pions; the fragmentation function into pions for these heavy particles will feature fewer pions at high z than for light quarks, and somewhat more pions with $z < 0.3$ or so. Secondly, QCD fragmentation functions depend to some degree on the energy scale of the process, whereas Equation 25 is scale-invariant.

An enhanced treatment of fragmentation and hadronization is possible using either more detailed QCD fragmentation functions or Monte Carlo simulations for the fragmentation and hadronization using parton shower codes like Pythia [32] or Herwig [33]. As we noted in Section 2.3, though, the function Equation 25 implies an average energy of final state photons and a multiplicity of final state photons per initial parton which match the $T_{BH}^{1/2}$

scaling of photon average energy and multiplicity found using a HERWIG-based Monte Carlo simulation for $1 \text{ GeV} \leq T_{\text{BH}} \leq 100 \text{ GeV}$ BH emission spectra [14]. We also showed in Section 2.6 that the time-integrated photon spectrum derived using the fragmentation function of Equation 25 is in good agreement with the parameterization of the time-integrated spectrum derived by fitting the results of the HERWIG-based Monte Carlo BH simulations. Thus the fragmentation function of 25 is adequate for deriving a good estimation of the overall instantaneous photon BH emission and power spectra in this work.

5.2. High-Energy Physics Beyond the Standard Model

The SEM is based on the Standard Model of high-energy physics, in which the Hawking-radiated fundamental quanta are limited to those whose existence has been confirmed in high-energy experiments: the photon, neutrinos, charged leptons, quarks, gluons, W and Z bosons, and the 125 GeV Higgs boson. There is strong evidence, however, that the Standard Model is incomplete. For example, observations of neutrino oscillations cannot be explained within the Standard Model and raise the question: are the neutrinos Dirac fermions (with 4 degrees of freedom for each of the 3 neutrino flavors) or Majorana fermions (with 2 degrees of freedom for each of the 3 neutrino flavors)? To date, only 6 neutrino degrees of freedom have been observed in detectors and so we assumed in our calculations that the neutrinos are Majorana fermions.

In theories beyond the Standard Model (BSM), other additional fundamental particle species may exist. For example, supersymmetry (SUSY) would imply the existence of SUSY partners for all the known Standard Model quanta - each $s = 1/2$ fundamental field would have an $s = 0$ superpartner field and each $s = 1$ fundamental field would have an $s = 1/2$ superpartner field. Other BSM theories that would introduce additional degrees of freedom include extra dimension theories implying massive Kaluza-Klein excitations of known fields; a shadow sector; and technicolor. In such models, the function $\alpha(M)$ will increase at each new rest mass threshold. The asymptotic rate of BH evaporation would thus be faster than the SEM rate and the remaining BH lifetime would be shorter. Additionally, the observable particle spectra may be modified, depending on the degree to which the new particle species couple to ordinary matter. Hence physics beyond the Standard Model may modify the details of the predictions for observations

of the final stages of PBH evaporation. If new degrees of freedom only manifest well above 100 TeV, however, there will be little overall change to our analysis.

5.2.1. Dirac Neutrinos

If neutrinos are Dirac fermions, the value of α must be modified. We can estimate the effect at high T_{BH} as follows. The total Hawking-radiated power determines the rate at which the BH mass decreases as the BH radiates particles. The function $\alpha(M_{BH})$, which is defined by Equation 11, accounts for the radiation of all relevant fundamental particle species by a black hole of mass M_{BH} . For the detection of the final gamma-ray burst from a BH, we are interested in remaining evaporation lifetimes in the range $\tau < 100$ s. Including the 6 extra degrees of freedom of Dirac neutrinos would increase the asymptotic ($\tau < 100$ s) value of $\alpha(M_{BH})$, which we took in our analysis to be α_{SM} , by 12% with little change to our analysis. We note, however, that if the extra Dirac neutrino degrees of freedom are light, $\alpha(M_{BH})$ would be increased at larger M_{BH} by a greater percentage. In particular, if the rest masses of the extra Dirac neutrino modes are lighter than ~ 100 MeV, the initial mass of a PBH whose lifetime equals the present age of the universe would be larger than the SEM value of 5×10^{11} kg by up to 15%.

5.2.2. Black Hole Emission with Supersymmetry

If there exists physics beyond the Standard Model (BSM), then any new BSM degrees of freedom should contribute to the Hawking radiation, changing the final BH evaporation rate and spectra. We now ask, would the contributions from new BSM particles be discernable at a VHE gamma-ray observatory, if the observatory observes a PBH burst event with a duration of order 100 s?

To elucidate the issues involved, we consider supersymmetry (SUSY) as our example of BSM physics. In typical SUSY models, such as the minimal supersymmetric standard model (MSSM), there are many new fundamental fields — essentially one superpartner for each known Standard Model field. Let us consider the case of a superpartner that is a squark of mass m_{sq} . Once $kT_{BH} \gtrsim T_{sq} \equiv m_{sq}c^2/x_{p,s=0}$, this squark species will appear in the Hawking radiation in significant numbers. The squark will then decay into a quark and other particles; the quark will next fragment into photons as described in Section 2, and the photons may be observed by the gamma-ray observatory.

Let τ_{sq} be the remaining burst lifetime when the black hole temperature reaches T_{sq} . If τ_{sq} is much larger than 100 s—the time window of the search—then a BH burst which includes squark emission cannot be distinguished from an SEM BH burst because the distance to the black hole is undetermined: an SEM BH burst would produce the same signal as a more distant BSM BH burst with squark radiation.

On the other hand, if the threshold time τ_{sq} is less than 100 s, the observatory would see an increase in the photon rate due to the squark radiation when the remaining BH evaporation lifetime becomes less than τ_{sq} . If the burst flux in the detector is large enough, the observatory may be sensitive to this photon rate increase.

In many SUSY models, such as those tested at the Large Hadron Collider, the rest masses of the superpartners are assumed to be of the order 500 GeV to 1 TeV, which would correspond to threshold times τ_{sq} much greater than 100 s. If the squark mass is of order 5 TeV, then $kT_{sq} = 1.9$ TeV and the threshold time τ_{sq} would occur during the time window of the PBH search. For a 5 TeV squark, the corresponding black hole mass threshold is

$$M_{BH,sq} = \hbar c^3 / (8\pi G_N k T_{sq}) = 5.5 \times 10^6 \text{ kg}. \quad (60)$$

The question of detector sensitivity to the squark-generated photons depends on the value of τ_{sq} when M_{BH} passes $M_{BH,sq}$. The remaining burst lifetime, in turn, depends on $\alpha(M_{BH})$. If we assume that the evaporation process is dominated by SEM particles until T_{BH} reaches T_{sq} , then

$$\alpha(M_{BH}) = \alpha_{SM} = 8.0 \times 10^{17} \text{ kg}^3 \text{ s}^{-1} \quad \text{for } M_{BH} > M_{BH,sq}. \quad (61)$$

For $M_{BH} < M_{BH,sq}$, $\alpha(M_{BH})$ increases by the contribution due to the squark

$$\alpha(M_{BH}) = \alpha_{SM} + \alpha_{sq} \quad \text{for } M < M_{BH,sq} \quad (62)$$

where the contribution from the squark degrees of freedom is,

$$\alpha_{sq} = 1.7 \times 10^{17} \text{ kg}^3 \text{ s}^{-1} \quad (63)$$

noting that the number of degrees of freedom for a squark with left-handed and right-handed states of the same mass is 12 (particle, antiparticle, handedness, and 3 colour modes) and $\Phi_{s=0} = 6.89$ for each squark degree of freedom.

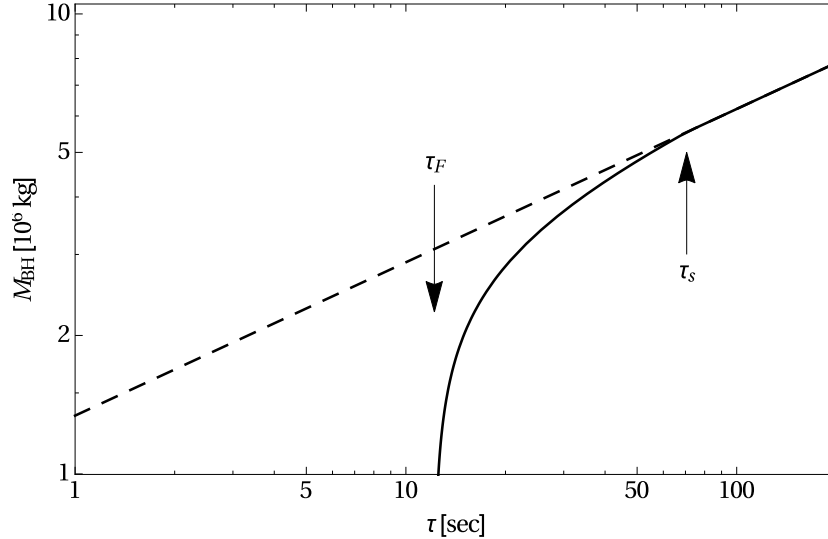


Figure 21: Black hole mass versus remaining burst lifetime. The time threshold for squark emission by the BSM BH is τ_{sq} ; the completion of the BSM BH burst occurs at τ_F . Solid curve: the BSM black hole with squark radiation. Dashed curve: the SEM black hole.

Figure 21 shows the masses of an SEM BH and the BSM BH as a function of the remaining lifetime τ of the SEM black hole, assuming for alignment purposes that both black holes had the same mass when $\tau \gg \tau_{sq}$. In this example, the threshold time for emission of the squark is $\tau_{sq} = 70$ s and the BSM BH burst expires at $\tau_F = 12$ s.

Figure 22 compares the rate of emission of fundamental particles as a function of time for a SEM BH and a BSM BH whose value of $\alpha(M_{BH})$ is given by Equation 62.

5.2.3. Statistical Estimate of Detection Sensitivity to Squark Emission

Let us make a rough estimate of the observational detector sensitivity to a SUSY squark threshold. As shown in Figure 20, a likely search interval for the HAWC observatory lies within the range of 10–100 s. The lowest squark mass which would fall within this search window range is then given by

$$m_{sq}c^2 \simeq 7.8x_{p,s=0} \left(\frac{1 \text{ s}}{\tau_{sq}} \right)^{1/3} \text{ TeV}. \quad (64)$$

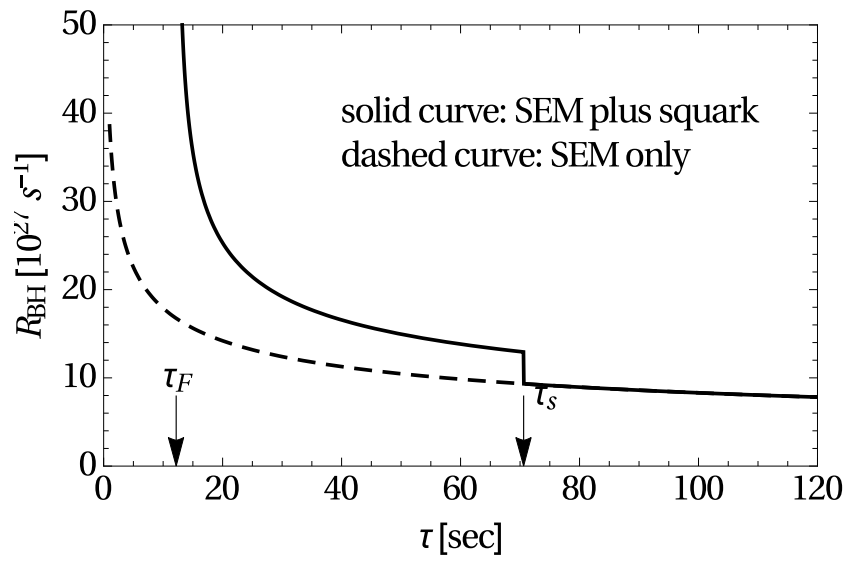


Figure 22: Black hole particle emission rate R versus remaining time. The time threshold for squark emission by the BSM BH is τ_{sq} ; the completion of the BSM BH burst occurs at τ_F . Solid curve: the BSM black hole with squark radiation. Dashed curve: the SEM black hole.

For $10 \text{ s} \lesssim \tau_{sq} \lesssim 100 \text{ s}$, this implies a squark rest mass range of $m_{sq}c^2 \simeq 5\text{--}10$ TeV. Because the value of α will increase due to the Hawking radiation of SUSY states, the actual remaining time will be somewhat shorter, and the squark mass range somewhat higher than this estimate.

The observational signature of a SUSY superpartner threshold being passed by the BH would be an enhanced photon rate at shorter remaining burst lifetimes (corresponding to $T_{BH} \geq T_{sq}$), compared to the rate at earlier times. To estimate the extent to which discerning such a rate enhancement is feasible, we consider the following conservative simplified model. A squark is expected to decay into a quark and the Lightest Supersymmetric Particle, typically a neutralino. If the neutralino mass is not a large fraction of the initial squark mass, then the quark should generate photons similar to those generated by a directly Hawking-radiated quark of the same initial energy as the squark. To count the number of degrees of freedom for the initial squark, we conservatively assume a squark of a single handedness because squark masses in general depend on handedness, i.e. here we will assume only 6 squark degrees of freedom (particle, antiparticle and 3 colors modes), rather than the 12 degrees of freedom used for α_{sq} in Equation 62). Recalling from Section 2.1 that $\Psi_{s=0} = 2.8\Psi_{s=1/2}$ and there are 72 total degrees of freedom for the $s = 1/2$ SEM quarks, we estimate that a squark degree of freedom is Hawking-radiated 2.8 more often than a quark degree of freedom when $T_{BH} > T_{sq}$. Thus the squark enhances the overall photon rate by a factor of $\sim 6 \times 2.8 \div 72 \simeq 23\%$.

In the same spirit, let us use a simple analysis to estimate the detectability of the photon rate change which occurs at τ_{sq} . Suppose that the power law of the BH photon burst emission time profile shown in Figure 12 is little changed after the SUSY superpartner threshold, i.e., we neglect any increase in α due to the SUSY states. Let us compare the number of photons in the last 10 seconds of the burst, with the number of photons seen in an earlier longer interval, say between 80 and 200 seconds prior to the end of the BH burst. The ratio is calculable in the SEM. Assuming the photon rate is enhanced by $\sim 20\%$ as estimated above for a squark threshold in the range $10 \text{ s} \lesssim \tau_{sq} \lesssim 80 \text{ s}$, the ratio in the SUSY model is also calculable. Applying the power law of Figure 12, the ratio of the number of photons in the 80-200 s interval is 0.97 times that in the 0-10 s interval for the SEM black hole, while it is 0.79 times that in the 0-10 s interval for the SUSY black hole. Taking the (optimistic) case considered in Figure 14 of a nearby PBH burst at 0.015 parsec whose final 10 seconds would produce a photon count

of ~ 1400 photons at the HAWC observatory, we find, considering Poisson fluctuations only in the number of signal photons and ignoring background fluctuations, that the SEM BH burst and a BSM BH burst with a squark threshold of $10 \text{ s} \lesssim \tau_{\text{sq}} \lesssim 80 \text{ s}$ would be distinguishable with a significance above 4 standard deviations.

Thus it is clear that detection of a nearby PBH burst has an interesting sensitivity to multi-TeV squark states which are currently inaccessible with hadron colliders. Further refinements of these calculations and other SUSY models will be presented in a separate paper.

5.3. Other Models of Strong Interaction Physics

The SEM assumes that relativistic quarks and gluons emitted as Hawking radiation escape as asymptotically free particles from their creation region close to the BH horizon (i.e., without strong interactions over distances up to of order 10^{-15} m appropriately Lorentz-transformed), analogous to quark and gluon jet creation in high-energy collisions in accelerator experiments. (See [3] for the details of this analogy.) Over distances of a few fermi appropriately Lorentz-transformed, the QCD quanta then undergo fragmentation and hadronization, consistent with observations of high energy accelerator collisions.

Some authors, however, have proposed that in the neighborhood of the BH the radiated particles undergo additional interactions. In these scenarios the Hawking radiation after emission self-interacts to form a dense photosphere around the microscopic black hole [40; 41; 42]. The emission rate is not modified but the particle energies are degraded to lower energies in the vicinity of the BH, resulting in a photon spectrum which, at high photon energies, would be less than that predicted by the SEM (Figure 5).

Recent detailed re-analysis of the published photosphere scenarios, however, has strongly argued that the conditions required for the production of intrinsically-induced photospheres are not met around Hawking-radiating black holes [3]. While models for intrinsically-produced photospheres do not seem viable, the possibility exists, however, in the SEM that the observable signal may be modified if the PBH is embedded in, for example, a region of ambient dense plasma or a strong magnetic field[3]. Although one should be cognizant that the above may change the observational characteristics and limits, we expect that the search methods will be primarily based on the SEM for the next generation of PBH searches.

5.4. PBH Evaporation Events in the Hagedorn Model

Some previous studies of black hole burst emission have assumed the Hagedorn model, also called the statistical bootstrap model. This particle physics model, which arose before the existence of quarks and gluons was confirmed in terrestrial accelerators, postulates that there is an exponentially rising spectrum of meson resonances once a threshold temperature Λ_{QCD} has been reached.

The Hagedorn PBH model assumes each of the meson resonances is an independent degree of freedom of Hawking radiation. Thus in the Hagedorn model, the function $\alpha(M_{BH})$ exponentially increases in this temperature regime and the PBH luminosity is correspondingly enhanced. The model also assumes that the remaining mass of the BH will be emitted around this temperature producing a stronger final burst that will be confined to lower photon energies ($\lesssim 1\text{GeV}$), in contrast to the SEM burst.

However, with the discovery of quark and gluon jets in accelerator collisions above Λ_{QCD} , the Hagedorn model is no longer a viable description of particle production in such collider events. Moreover, detailed consideration [3] of the particle separation, energies and timescales of Hawking radiation of QCD particles, indicates that the asymptotic freedom of QCD, which describes jet production at hadron colliders, applies to Hawking radiation, rather than meson resonance or quark-gluon plasma production. Additionally, because the Hawking radiation of a particle correspondingly reduces the BH mass and hence increases the BH temperature, any Hagedorn phase can at most be temporary with the BH transitioning quickly to temperatures above the Hagedorn regime. The form of the absorption factor Γ of Equation 1 also strongly suppresses the Hawking emission of a species when TBH is close to the rest mass threshold of the species, i.e., in this case, weakening the signal from any temporary Hagedorn regime. Taken together, these considerations strongly argue against the Hagedorn model applying to BH emission or producing an enhanced PBH burst signal at the detector.

5.5. Do Very Short Gamma-ray Bursts Originate from PBHs?

Studies of very short gamma-ray bursts (VSGRB), with time durations $\lesssim 0.1$ s, tentatively suggest that these events may form a distinct class of GRBs [43; 44]. The data used in these studies come from BATSE, Fermi GBM, Swift, KONUS, and other keV/MeV gamma-ray detectors [43; 45]. Evidence that the VSGRBs are distinctly different from GRBs of longer duration includes the anisotropy on the sky of the distribution of VSGRBs [44]

and the hardness of their photon spectra. The VSGRB sky positions may be clustered closed to the anti-galactic center region [44], unlike short or long GRBs, possibly indicating that the VSGRBs may have local origin.

These characteristics of VSGRBs have led to speculation that some fraction of these events may be PBH bursts [43; 46]. The photon energies of these detectors are much lower than the 50 GeV – 100 TeV range considered in Section 2. The highest photon energies observed in these VSGRBs are less than 10 MeV. The authors in Ref. [43] suggest that enhanced BH emission may occur when the BH temperature approaches the QCD phase transition Λ_{QCD} , i.e., $T_{\text{BH}} \approx 100$ MeV. It is possible that the VSGRBs may ultimately be explained by astronomical processes involving compact objects such as neutron stars in the Milky Way galaxy. In any case, PBH searches at TeV-scale observatories will be based on the SEM at $T_{\text{BH}} \gg 100$ MeV.

6. Summary and Conclusions

In this paper, we have reviewed and analyzed the theoretical framework of the standard BH emission mechanism and explored observational characteristics of the final burst. Moreover we have also explored and compared PBH burst search methods and differences between PBH burst and standard cosmological GRBs. Here are the main finding and conclusions of this paper:

1. We have developed improved approximate analytical formulae for the instantaneous BH photon spectrum which includes both the directly Hawking-radiated photons and the photons resulting from the decay or fragmentation and hadronization of other directly Hawking-radiated species. Our analysis incorporates the most recent LHC Standard Model results.
2. For the first time, we have calculated the PBH burst light curve (time profile) and studied its energy dependence both at the source and at the detector.
3. At low energies ($E_\gamma < 10$ TeV), the PBH burst light curve time profile does not show much variation with energy and is well described as a function of remaining burst lifetime by a power law of index ~ -0.7 . However, at high energies, the PBH burst light curve profile displays significant variation with energy that may be used as an unique signature of PBH bursts. In addition, at high energies, the light curve profile shows an inflection region around 0.1 seconds. The HAWC observatory

is sensitive in this energy range for a sufficiently nearby PBH and the above features in the light curve may be used to uniquely identify PBH bursts.

4. Compared to the burst Simple Search (photon counting) method, we have found that Maximum Likelihood search methods using the PBH burst light curve are about 30% more sensitive to PBH bursts. However, we also found that there is not a significant difference in sensitivity between 10 bin Maximum Likelihood searches and unbinned Maximum Likelihood searches.
5. We have discussed in Section 4 the expected differences between PBH bursts and standard cosmological GRBs, in particular that the PBH bursts evolve higher into the TeV band and are typically not expected to be accompanied by an afterglow.
6. We have shown in Section 5.2 the possibility that evidence of beyond the Standard Model (BSM) physics may be discernible in the detector signature of a PBH burst. In particular, a squark state with a rest mass of 5-10 TeV is expected to produce a detectable change in the time dependence of the arrival rate of TeV photons emitted in the final 200 seconds of the PBH burst.

7. Acknowledgements

This work was supported by grants from the National Science Foundation (MSU) and Department of Energy (LANL). TNU acknowledges the partial support of this work by the Laboratory Directed Research & Development (LDRD) program at LANL. We would also like to thank Wade Fisher of MSU for useful conversations on the likelihood fits, Jing-Ya Zhu of MSU for discussions on current models of supersymmetry and Sekhar Chivukula of MSU for useful conversations on Higgs field degrees of freedom.

References

- [1] B. J. Carr, K. Kohri, Y. Sendouda, and J. Yokoyama, “New cosmological constraints on primordial black holes,” *Phys. Rev. D*, vol. 81, p. 104019, May 2010.
- [2] S. W. Hawking, “Black hole explosions?,” *Nature*, vol. 248, pp. 30–31, Mar. 1974.

- [3] J. H. MacGibbon, B. J. Carr, and D. N. Page, “Do evaporating black holes form photospheres?,” *Phys. Rev. D*, vol. 78, p. 064043, Sept. 2008.
- [4] F. Halzen, E. Zas, J. H. MacGibbon, and T. C. Weekes, “Gamma rays and energetic particles from primordial black holes,” *Nature*, vol. 353, pp. 807–815, Oct. 1991.
- [5] K. Griest, M. J. Lehner, A. M. Cieplak, and B. Jain, “Microlensing of Kepler Stars as a Method of Detecting Primordial Black Hole Dark Matter,” *Physical Review Letters*, vol. 107, p. 231101, Dec. 2011.
- [6] A. P. Trofimenko, “Black holes in cosmic bodies,” *Ap&SS*, vol. 168, pp. 277–292, June 1990.
- [7] D. E. Alexandreas, G. E. Allen, D. Berley, S. Biller, R. L. Burman, M. Cavalli-Sforza, C. Y. Chang, M. L. Chen, P. Chumney, D. Coyne, C. Dion, G. M. Dion, D. Dorfan, R. W. Ellsworth, J. A. Goodman, T. J. Haines, M. Harmon, C. M. Hoffman, L. Kelley, S. Klein, D. E. Nagle, D. M. Schmidt, R. Schnee, C. Sinnis, A. Shoup, M. J. Stark, D. D. Weeks, D. A. Williams, J. P. Wu, T. Yang, G. B. Yodh, and W. P. Zhang, “New limit on the rate-density of evaporating black holes,” *Physical Review Letters*, vol. 71, pp. 2524–2527, Oct. 1993.
- [8] M. Amenomori, Z. Cao, B. Z. Dai, L. K. Ding, Y. X. Feng, Z. Y. Feng, K. Hibino, N. Hotta, Q. Huang, A. X. Huo, H. Y. Jia, G. Z. Jiang, S. Q. Jiao, F. Kajino, K. Kasahara, Y. Kitahara, Labaciren, S. M. Liu, D. M. Mei, L. Meng, X. R. Meng, Mimaciren, K. Mizutani, J. Mu, H. Nanjo, M. Nishizawa, A. Oguro, M. Ohnishi, I. Ohta, T. Ouchi, J. R. Ren, T. Saito, M. Sakata, Z. Z. Shi, M. Shibata, T. Shirai, H. Sugimoto, X. X. Sun, K. Taira, Y. H. Tan, N. Tateyama, S. Torii, H. Wang, C. Z. Wen, Y. Yamamoto, G. C. Yu, P. Yuan, C. S. Zhang, H. M. Zhang, L. Zhang, Zhasang, Zhaxiciren, and W. D. Zhou, “Search for 10 TeV Gamma Bursts from Evaporating Primordial Black Holes with the Tibet Air Shower Array,” *International Cosmic Ray Conference*, vol. 2, p. 112, 1995.
- [9] E. T. Linton, R. W. Atkins, H. M. Badran, G. Blaylock, P. J. Boyle, J. H. Buckley, K. L. Byrum, D. A. Carter-Lewis, O. Celik, Y. C. K. Chow, P. Cogan, M. K. Daniel, C. Dowdall, A. D. Falcone, D. J. Fegan, S. J. Fegan, J. P. Finley, P. Fortin, K. J. Guiterrez, J. Hall, D. Hanna,

- J. Holder, D. Horan, S. B. Hughes, T. B. Humensky, I. Jung, G. E. Kenny, M. Kertzman, D. B. Kieda, J. Kildea, J. Knapp, H. Krawczynski, M. J. Lang, S. LeBohec, G. Maier, P. Moriarty, R. A. Ong, J. S. Perkins, F. Pizlo, M. Pohl, J. Quinn, K. Ragan, P. F. Rebillot, P. T. Reynolds, G. H. Sembroski, D. Steele, S. P. Swordy, L. Valcarcel, S. P. Wakely, T. C. Weekes, and R. J. White, “A new search for primordial black hole evaporations using the Whipple gamma-ray telescope,” *JCAP*, vol. 1, p. 13, Jan. 2006.
- [10] G. Tešić and VERITAS Collaboration, “Searching for primordial black holes with the VERITAS gamma-ray experiment,” *Journal of Physics Conference Series*, vol. 375, p. 052024, July 2012.
- [11] J. Glicenstein, A. Barnacka, M. Vivier, T. Herr, and for the H. E. S. S. Collaboration, “Limits on Primordial Black Hole evaporation with the H.E.S.S. array of Cherenkov telescopes,” *ArXiv e-prints 1307.4898*, July 2013.
- [12] T. U. Ukwatta, D. Stump, J. T. Linnemann, K. Tollefson, V. Vasileiou, G. Sinnis, and J. H. MacGibbon, “Milagro Limits on the Rate-Density of Primordial Black Holes,” *7th Huntsville Gamma-Ray Burst Symposium, GRB 2013: paper 44 in eConf Proceedings C1304143*, Aug. 2013.
- [13] A. A. Abdo, A. U. Abeysekara, R. Alfaro, B. T. Allen, C. Alvarez, J. D. Álvarez, R. Arceo, J. C. Arteaga-Velázquez, T. Aune, H. A. Ayala Solares, A. S. Barber, B. M. Baughman, N. Bautista-Elivar, J. Berra Gonzalez, E. Belmont, S. Y. BenZvi, D. Berley, M. Bonilla Rosales, J. Braun, R. A. Caballero-Lopez, K. S. Caballero-Mora, A. Carramiñana, M. Castillo, G. E. Christopher, U. Cotti, J. Cotzomi, E. de la Fuente, C. De León, T. DeYoung, R. Diaz Hernandez, L. Diaz-Cruz, J. C. Díaz-Vélez, B. L. Dingus, M. A. DuVernois, R. W. Ellsworth, D. W. Fiorino, N. Fraija, A. Galindo, F. Garfias, M. M. González, J. A. Goodman, V. Grabski, M. Gussert, Z. Hampel-Arias, J. P. Harding, E. Hays, C. M. Hoffman, C. M. Hui, P. Hütemeyer, A. Imran, A. Iriarte, P. Karn, D. Kieda, B. E. Kolterman, G. J. Kunde, A. Lara, R. J. Lauer, W. H. Lee, D. Lennarz, H. León Vargas, E. C. Linares, J. T. Linnemann, M. Longo, R. Luna-García, J. H. MacGibbon, A. Marinelli, S. S. Marinelli, H. Martinez, O. Martinez, J. Martínez-Castro, J. A. J.

- Matthews, J. McEnery, E. Mendoza Torres, A. I. Mincer, P. Miranda-Romagnoli, E. Moreno, T. Morgan, M. Mostafá, L. Nellen, P. Nemethy, M. Newbold, R. Noriega-Papaqui, T. Ocegüera-Becerra, B. Patricelli, R. Pelayo, E. G. Pérez-Pérez, J. Pretz, C. Rivière, D. Rosa-González, E. Ruiz-Velasco, J. Ryan, H. Salazar, F. Salesa, A. Sandoval, P. M. Saz Parkinson, M. Schneider, S. Silich, G. Sinnis, A. J. Smith, D. Stump, K. Sparks Woodle, R. W. Springer, I. Taboada, P. A. Toale, K. Tollefson, I. Torres, T. N. Ukwatta, V. Vasileiou, L. Villaseñor, T. Weisgarber, S. Westerhoff, D. A. Williams, I. G. Wisher, J. Wood, G. B. Yodh, P. W. Younk, D. Zaborov, A. Zepeda, and H. Zhou, “Milagro limits and HAWC sensitivity for the rate-density of evaporating Primordial Black Holes,” *Astroparticle Physics*, vol. 64, pp. 4–12, Apr. 2015.
- [14] J. H. MacGibbon and B. R. Webber, “Quark- and gluon-jet emission from primordial black holes: The instantaneous spectra,” *Phys. Rev. D*, vol. 41, pp. 3052–3079, May 1990.
- [15] M. W. E. Smith, D. B. Fox, D. F. Cowen, P. Mészáros, G. Tešić, J. Fixelle, I. Bartos, P. Sommers, A. Ashtekar, G. Jogesh Babu, S. D. Barthelmy, S. Coutu, T. DeYoung, A. D. Falcone, S. Gao, B. Hashemi, A. Homeier, S. Márka, B. J. Owen, and I. Taboada, “The Astrophysical Multimessenger Observatory Network (AMON),” *Astroparticle Physics*, vol. 45, pp. 56–70, May 2013.
- [16] S. W. Hawking, “Particle Creation by Black Holes,” *Commun. math. Phys.*, vol. 43, pp. 199–220, 1975.
- [17] D. N. Page, “Particle emission rates from a black hole. II - Massless particles from a rotating hole,” *Phys. Rev. D*, vol. 14, pp. 3260–3273, Dec. 1976.
- [18] D. N. Page, “Particle emission rates from a black hole. III - Charged leptons from a nonrotating hole,” *Phys. Rev. D*, vol. 16, pp. 2402–2411, Oct. 1977.
- [19] D. N. Page, “Particle emission rates from a black hole: Massless particles from an uncharged, nonrotating hole,” *Phys. Rev. D*, vol. 13, pp. 198–206, Jan. 1976.

- [20] T. Elster, “Polarisation of the vacuum near a black hole inside a spherical cavity,” *Journal of Physics A Mathematical General*, vol. 16, pp. 989–996, Apr. 1983.
- [21] T. Elster, “Vacuum polarization near a black hole creating particles,” *Physics Letters A*, vol. 94, pp. 205–209, Mar. 1983.
- [22] R. D. Simkins, *Massive scalar particle emission from Schwarzschild black holes*. PhD thesis, Pennsylvania State University, University Park., 1986.
- [23] J. Beringer, J.-F. Arguin, R. M. Barnett, K. Copic, O. Dahl, D. E. Groom, C.-J. Lin, J. Lys, H. Murayama, C. G. Wohl, W.-M. Yao, P. A. Zyla, C. Amsler, M. Antonelli, D. M. Asner, H. Baer, H. R. Band, T. Basaglia, C. W. Bauer, J. J. Beatty, V. I. Belousov, E. Bergren, G. Bernardi, W. Bertl, S. Bethke, H. Bichsel, O. Biebel, E. Blucher, S. Blusk, G. Brooijmans, O. Buchmueller, R. N. Cahn, M. Carena, A. Ceccucci, D. Chakraborty, M.-C. Chen, R. S. Chivukula, G. Cowan, G. D’Ambrosio, T. Damour, D. de Florian, A. de Gouvêa, T. DeGrand, P. de Jong, G. Dissertori, B. Dobrescu, M. Doser, M. Drees, D. A. Edwards, S. Eidelman, J. Erler, V. V. Ezhela, W. Fetscher, B. D. Fields, B. Foster, T. K. Gaiser, L. Garren, H.-J. Gerber, G. Gerbier, T. Gherghetta, S. Golwala, M. Goodman, C. Grab, A. V. Gritsan, J.-F. Grivaz, M. Grünewald, A. Gurtu, T. Gutsche, H. E. Haber, K. Hagiwara, C. Hagmann, C. Hanhart, S. Hashimoto, K. G. Hayes, M. Heffner, B. Heltsley, J. J. Hernández-Rey, K. Hikasa, A. Höcker, J. Holder, A. Holtkamp, J. Huston, J. D. Jackson, K. F. Johnson, T. Junk, D. Karlen, D. Kirkby, S. R. Klein, E. Klempt, R. V. Kowalewski, F. Krauss, M. Kreps, B. Krusche, Y. V. Kuyanov, Y. Kwon, O. Lahav, J. Laiho, P. Langacker, A. Liddle, Z. Ligeti, T. M. Liss, L. Littenberg, K. S. Lugovsky, S. B. Lugovsky, T. Mannel, A. V. Manohar, W. J. Marciano, A. D. Martin, A. Masoni, J. Matthews, D. Milstead, R. Miquel, K. Mönig, F. Moortgat, K. Nakamura, M. Narain, P. Nason, S. Navas, M. Neubert, P. Nevski, Y. Nir, K. A. Olive, L. Pape, J. Parsons, C. Patrignani, J. A. Peacock, S. T. Petcov, A. Piepke, A. Pomarol, G. Punzi, A. Quadt, S. Raby, G. Raffelt, B. N. Ratcliff, P. Richardson, S. Roesler, S. Rolli, A. Romaniouk, L. J. Rosenberg, J. L. Rosner, C. T. Sachrajda, Y. Sakai, G. P. Salam, S. Sarkar, F. Sauli, O. Schneider, K. Scholberg, D. Scott, W. G. Seligman, M. H. Shaevitz, S. R. Sharpe, M. Silari, T. Sjöstrand, P. Skands, J. G. Smith, G. F. Smoot, S. Spanier,

- H. Spieler, A. Stahl, T. Stanev, S. L. Stone, T. Sumiyoshi, M. J. Syphers, F. Takahashi, M. Tanabashi, J. Terning, M. Titov, N. P. Tkachenko, N. A. Törnqvist, D. Tovey, G. Valencia, K. van Bibber, G. Venanzoni, M. G. Vincter, P. Vogel, A. Vogt, W. Walkowiak, C. W. Walter, D. R. Ward, T. Watari, G. Weiglein, E. J. Weinberg, L. R. Wiencke, L. Wolfenstein, J. Womersley, C. L. Woody, R. L. Workman, A. Yamamoto, G. P. Zeller, O. V. Zenin, J. Zhang, R.-Y. Zhu, G. Harper, V. S. Lugovsky, and P. Schaffner, “Review of Particle Physics,” *Phys. Rev. D*, vol. 86, p. 010001, July 2012.
- [24] G. Aad, B. Abbott, J. Abdallah, and et. al., “Combined Measurement of the Higgs Boson Mass in pp Collisions at $\sqrt{s}=7$ and 8 TeV with the ATLAS and CMS Experiments,” *Phys. Rev. Lett.*, vol. 114, p. 191803, May 2015.
- [25] M. S. Chanowitz, “Electroweak symmetry breaking: unitarity, dynamics, and experimental prospects,” *Annual Review of Nuclear and Particle Science*, vol. 38, pp. 323–420, 1988.
- [26] M. J. Perry, “Black holes are coloured,” *Physics Letters B*, vol. 71, pp. 234–236, Nov. 1977.
- [27] D. N. Page, B. J. Carr, and J. H. MacGibbon, “Bremsstrahlung effects around evaporating black holes,” *Phys. Rev. D*, vol. 78, p. 064044, Sept. 2008.
- [28] D. de Florian, R. Sassot, and M. Stratmann, “Global analysis of fragmentation functions for protons and charged hadrons,” *Phys. Rev. D*, vol. 76, p. 074033, Oct. 2007.
- [29] S. Albino, B. A. Kniehl, and G. Kramer, “AKK update: Improvements from new theoretical input and experimental data,” *Nuclear Physics B*, vol. 803, pp. 42–104, Nov. 2008.
- [30] C. T. Hill, “Monopolonium,” *Nuclear Physics B*, vol. 224, pp. 469–490, Sept. 1983.
- [31] C. T. Hill, D. N. Schramm, and T. P. Walker, “Ultra-high-energy cosmic rays from superconducting cosmic strings,” *Phys. Rev. D*, vol. 36, pp. 1007–1016, Aug. 1987.

- [32] T. Sjöstrand, S. Mrenna, and P. Skands, “A brief introduction to PYTHIA 8.1,” *Computer Physics Communications*, vol. 178, pp. 852–867, June 2008.
- [33] J. Bellm, S. Gieseke, D. Grellscheid, A. Papaefstathiou, S. Platzer, P. Richardson, C. Rohr, T. Schuh, M. H. Seymour, A. Siodmok, A. Wilcock, and B. Zimmermann, “Herwig++ 2.7 Release Note,” *ArXiv 1310.6877*, Oct. 2013.
- [34] E. Bugaev, P. Klimai, and V. Petkov, “Photon spectra from final stages of a primordial black hole evaporation in different theoretical models,” *International Cosmic Ray Conference*, vol. 3, pp. 1123–1126, 2008.
- [35] V. B. Petkov, E. V. Bugaev, P. A. Klimai, M. V. Andreev, V. I. Volchenko, G. V. Volchenko, A. N. Gaponenko, Z. S. Guliev, I. M. Dzaparova, D. V. Smirnov, A. V. Sergeev, A. B. Chernyaev, and A. F. Yanin, “Searching for very-high-energy gamma-ray bursts from evaporating primordial black holes,” *Astronomy Letters*, vol. 34, pp. 509–514, Aug. 2008.
- [36] HAWC Collaboration, A. U. Abeysekara, R. Alfaro, C. Alvarez, J. D. Álvarez, R. Arceo, J. C. Arteaga-Velázquez, H. A. Ayala Solares, A. S. Barber, B. M. Baughman, N. Bautista-Elivar, E. Belmont, S. Y. BenZvi, D. Berley, M. Bonilla Rosales, J. Braun, R. A. Caballero-Lopez, K. S. Caballero-Mora, A. Carramiñana, M. Castillo, U. Cotti, J. Cotzomi, E. de la Fuente, C. De León, T. DeYoung, R. Diaz Hernandez, J. C. Díaz-Vélez, B. L. Dingus, M. A. DuVernois, R. W. Ellsworth, A. Fernandez, D. W. Fiorino, N. Fraija, A. Galindo, F. Garfias, L. X. González, M. M. González, J. A. Goodman, V. Grabski, M. Gussert, Z. Hampel-Arias, C. M. Hui, P. Hütemeyer, A. Imran, A. Iriarte, P. Karn, D. Kieda, G. J. Kunde, A. Lara, R. J. Lauer, W. H. Lee, D. Lennarz, H. León Vargas, E. C. Linares, J. T. Linnemann, M. Longo, R. Luna-García, A. Marinelli, H. Martinez, O. Martinez, J. Martínez-Castro, J. A. J. Matthews, P. Miranda-Romagnoli, E. Moreno, M. Mostafá, J. Nava, L. Nellen, M. Newbold, R. Noriega-Papaqui, T. Ocegüera-Becerra, B. Patricelli, R. Pelayo, E. G. Pérez-Pérez, J. Pretz, C. Rivière, D. Rosa-González, H. Salazar, F. Salesa, F. E. Sanchez, A. Sandoval, E. Santos, M. Schneider, S. Silich, G. Sinnis, A. J. Smith, K. Sparks, R. W. Springer, I. Taboada, P. A. Toale, K. Tollefson, I. Torres, T. N. Ukwatta,

- L. Villaseñor, T. Weisgarber, S. Westerhoff, I. G. Wisher, J. Wood, G. B. Yodh, P. W. Younk, D. Zaborov, A. Zepeda, and H. Zhou, “The HAWC Gamma-Ray Observatory: Dark Matter, Cosmology, and Fundamental Physics,” *ArXiv 1310.0073*, Sept. 2013.
- [37] M. G. Hauser and E. Dwek, “The Cosmic Infrared Background: Measurements and Implications,” *ARA&A*, vol. 39, pp. 249–307, 2001.
- [38] MAGIC Collaboration, J. Albert, E. Aliu, H. Anderhub, L. A. Antonelli, P. Antoranz, M. Backes, C. Baixeras, J. A. Barrio, H. Bartko, D. Bastieri, J. K. Becker, W. Bednarek, K. Berger, E. Bernardini, C. Bigongiari, A. Biland, R. K. Bock, G. Bonnoli, P. Bordas, V. Bosch-Ramon, T. Bretz, I. Britvitch, M. Camara, E. Carmona, A. Chilingarian, S. Commichau, J. L. Contreras, J. Cortina, M. T. Costado, S. Covino, V. Curtef, F. Dazzi, A. De Angelis, E. D. Cea del Pozo, R. de los Reyes, B. De Lotto, M. De Maria, F. De Sabata, C. D. Mendez, A. Dominguez, D. Dorner, M. Doro, M. Errando, M. Fagiolini, D. Ferenc, E. Fernández, R. Firpo, M. V. Fonseca, L. Font, N. Galante, R. J. García López, M. Garczarczyk, M. Gaug, F. Goebel, M. Hayashida, A. Herrero, D. Höhne, J. Hose, C. C. Hsu, S. Huber, T. Jogler, T. M. Kneiske, D. Kranich, A. La Barbera, A. Laille, E. Leonardo, E. Lindfors, S. Lombardi, F. Longo, M. López, E. Lorenz, P. Majumdar, G. Maneva, N. Mankuzhiyil, K. Mannheim, L. Maraschi, M. Mariotti, M. Martínez, D. Mazin, M. Meucci, M. Meyer, J. M. Miranda, R. Mirzoyan, S. Mizobuchi, M. Moles, A. Moralejo, D. Nieto, K. Nilsson, J. Ninkovic, N. Otte, I. Oya, M. Panniello, R. Paoletti, J. M. Paredes, M. Pasanen, D. Pascoli, F. Paus, R. G. Pegna, M. A. Perez-Torres, M. Persic, L. Peruzzo, A. Piccioli, F. Prada, E. Prandini, N. Puchades, A. Raymers, W. Rhode, M. Ribó, J. Rico, M. Rissi, A. Robert, S. Rügamer, A. Saggion, T. Y. Saito, M. Salvati, M. Sanchez-Conde, P. Sartori, K. Satalecka, V. Scalzotto, V. Scapin, R. Schmitt, T. Schweizer, M. Shayduk, K. Shinozaki, S. N. Shore, N. Sidro, A. Sierpowska-Bartosik, A. Sillanpää, D. Sobczynska, F. Spanier, A. Stamerra, L. S. Stark, L. Takalo, F. Tavecchio, P. Temnikov, D. Tesaro, M. Teshima, M. Tluczykont, D. F. Torres, N. Turini, H. Vankov, A. Venturini, V. Vitale, R. M. Wagner, W. Wittek, V. Zabalza, F. Zandanel, R. Zanin, and J. Zapatero, “Very-High-Energy gamma rays from a Distant Quasar: How Transparent Is the Universe?,” *Science*, vol. 320, p. 1752, June 2008.

- [39] F. Halzen, B. Keszthelyi, and E. Zas, “Neutrinos from primordial black holes,” *Phys. Rev. D*, vol. 52, pp. 3239–3247, Sept. 1995.
- [40] A. F. Heckler, “Formation of a Hawking-radiation photosphere around microscopic black holes,” *Phys. Rev. D*, vol. 55, pp. 480–488, Jan. 1997.
- [41] A. F. Heckler, “Calculation of the Emergent Spectrum and Observation of Primordial Black Holes,” *Physical Review Letters*, vol. 78, pp. 3430–3433, May 1997.
- [42] J. Kapusta, “The Last Eight Minutes of a Primordial Black Hole,” *astro-ph/9911309*, Nov. 1999.
- [43] D. B. Cline, B. Czerny, C. Matthey, A. Janiuk, and S. Otwinowski, “Study of Very Short Gamma-Ray Bursts: New Results from BATSE and Konus,” *ApJ. Lett.*, vol. 633, pp. L73–L76, Nov. 2005.
- [44] T. N. Ukwatta and P. R. Wozniak, “Investigation of Redshift- and Duration-Dependent Clustering of Gamma-ray Bursts,” *ArXiv e-prints arXiv:1507.07117*, July 2015.
- [45] D. B. Cline, “Do Very Short Gamma Ray Bursts Originate from Primordial Black Holes? Review,” *International Journal of Astronomy and Astrophysics*, vol. 1, pp. 164–172, 2011.
- [46] B. Czerny, A. Janiuk, D. B. Cline, and S. Otwinowski, “Observational constraints on the nature of very short gamma-ray bursts,” *New Astronomy*, vol. 16, pp. 33–45, Jan. 2011.